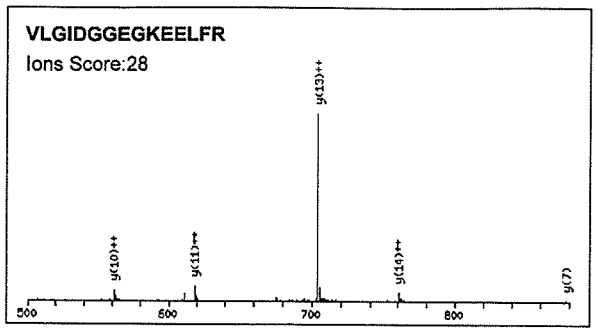

(1) MS² spectrum

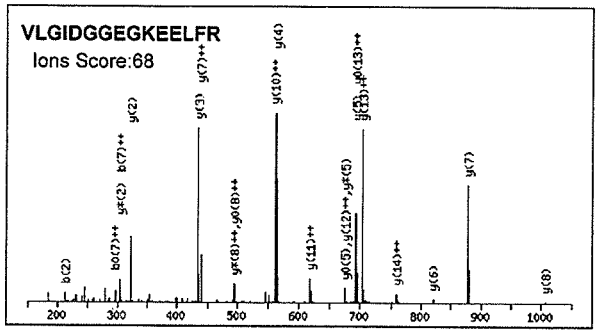

(2) MS² and MS³ spectrum

Figure 9. Example of analyzing MS^3.

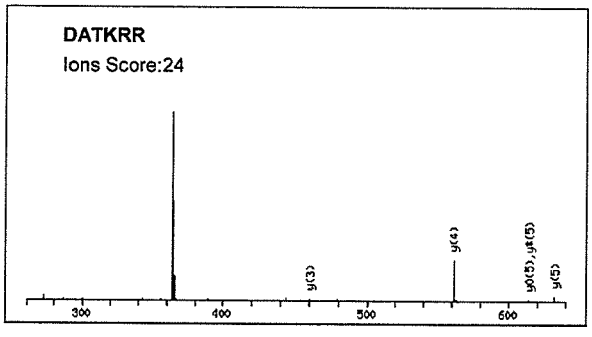

(1) MS² spectrum

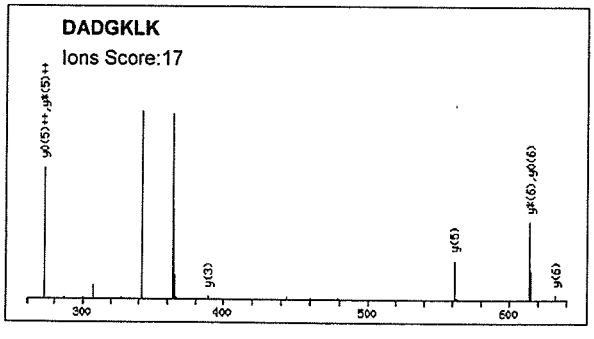

(2) MS² and MS³ spectrum

Figure 10. Example of analyzing MS^3.

Furthermore, in the case where the score decreases though volume of information has obviously increased with auto MS^3 analysis, there is a possibility that the amino acid sequence was modified posttranslationally or not registered in the protein database. For these cases, the change of the database searching condition or analysis using *de novo* sequencing is effective.

CONCLUSIONS

We have installed the software, based on our method, on a modified prototype model of a nanoLC/ion-Trap/oaTOF mass spectrometer equipped with an ESI source. We applied it to a high-protein mixture as a target sample and checked the fundamental functions from the results. The following results were obtained.

- The total processing time to evaluate raw MS and raw MS^2 data for optimization by tandem mass spectrometry is less than 10 ms, which is the setup time of the next MS^2 acquisition.
- The charge states of 90% of precursor ions are correctly identified in real time by this method.
- The total number of identified proteins in five runs was higher by a factor of 3.3 compared to that in the first run.
- The ion scores for peptide identification increase significantly in about 70% of cases when the MS^3 spectra, combined with MS^2 spectra before being subjected to Mascot® analysis, are used.

Therefore, the real-time optimization technique for tandem mass spectrometry is feasible and useful to detect low-abundance proteins with high throughput and high accuracy in highly complex protein mixtures.

Acknowledgement

We thank Dr. Yoshiya Oda of Eisai Co., Ltd. for fruitful discussions. We also acknowledge Naomi Manri and Masako Ishimaru for their invaluable assistance with these experiments and the financial support provided by Hitachi High Technologies, Ltd. This work was supported by the New Energy and Industrial Technology Development Organization (NEDO), Japan.

REFERENCES

1. Perkins DN, Pappin DJC, Creasy DM, Cottrell JS. *Electrophoresis* 1999; **20**: 3551.
2. Eng JK, McCormack AL, Yates JR III. *J. Am. Soc. Mass Spectrom.* 1994; **5**: 976.
3. Biemann K, Martin SA. *Mass Spectrom. Rev.* 1987; **6**: 1.
4. McCormack AL, Somogyi A, Dongre AR, Wysocki VH. *Anal. Chem.* 1993; **65**: 2859.
5. Wysocki VH, Tsaprailis G, Smith LL, Breci LA. *J. Mass Spectrom.* 2000; **35**: 1399.
6. Tabb DL, Huang Y, Wysocki VH, Yates JR III. *Anal. Chem.* 2004; **76**: 1243.
7. Cu C, Somogyi A, Wysocki VH, Medzihradszky KF. *Anal. Chim. Acta* 1999; **397**: 247.
8. Kapp EA, Schutz F, Reid GE, Eddes JS, Moritz RL, O'Hair RAJ, Speed TP, Simpson RJ. *Anal. Chem.* 2003; **75**: 6251.
9. Mohammed S, Chalmers MJ, Gielbert J, Ferro M, Gora L, Smith DC, Gaskell SJ. *J. Mass Spectrom.* 2001; **26**: 1260.
10. Mann M, Wilm M. *Anal. Chem.* 1994; **66**: 4390.
11. Horn DM, Zubarev RA, McLafferty FW. *Proc. Natl. Acad. Sci.* 2000; **97**: 10313.
12. Searle BC, Dasari S, Turner M, Reddy AP, Choi D, Wilmarth PA, McCormack AL, David LL, Nagalla SR. *Anal. Chem.* 2004; **76**: 2220.
13. Shevchenko A, Ghernushevich I, Ens W, Standing KG, Thomson B, Wilm M, Mann M. *Rapid Commun. Mass Spectrom.* 1997; **11**: 1015.
14. Fernandez-de-Cossio J, Gonzalez J, Betancourt L, Besada V, Padron G, Shimonishi Y, Takao T. *Rapid Commun. Mass Spectrom.* 1998; **12**: 1867.

DOI: 10.1002/rcm

FEBS Letters 580 (2006) 199–205

Evidence for phosphorylation of rat liver glucose-regulated protein 58, GRP58/ERp57/ER-60, induced by fasting and leptin

Kanako Kita, Nobuaki Okumura, Toshifumi Takao, Makoto Watanabe, Toshiya Matsubara, Osamu Nishimura, Katsuya Nagai*

Laboratory of Proteins Involved in Homeostatic Integration, Institute for Protein Research, Osaka University, 3-2, Yamada-Oka, Suita, Osaka 565-0871, Japan

Received 8 November 2005; revised 28 November 2005; accepted 29 November 2005

Available online 9 December 2005

Edited by Gianni Cesareni

Abstract **Glucose-regulated protein 58 (GRP58)-like immunoreactivity in rat liver obtained in the evening or after fasting underwent an electrophoretic band-shift, which disappeared after phosphatase-treatment. Since mass spectrometric analysis raised a possibility that Ser150 of GRP58 is phosphorylated, an antibody against the phosphoserine150 GRP58 was generated. Immunoreactivity to this antibody was increased in the evening and after fasting. Since GRP58 was shown to interact with signal transducer and activator of transduction 3 (STAT3), a leptin-related protein, the effect of leptin was examined. Immunoreactivity to the anti-phosphoGRP58 antibody was markedly elevated after the leptin injection, indicating that Ser150 of GRP58 is phosphorylated after fasting and leptin-treatment.**

Keywords: GRP58; ERp57; MALDI-TOF-MS; Alkaline phosphatase; Hydrogen fluoride; Fasting; STAT3; Phosphorylation

1. Introduction

To investigate daily changes in liver function, protein expression patterns in the rat liver were analyzed by proteome analysis using one- and two-dimensional electrophoresis (1DE and 2DE), mass spectrometry and immunoblotting. Multiple spots of immunoreactivity to an anti-glucose-regulated protein 58 (GRP58) antibody were detected. GRP58 is a stress protein of about 60 k whose expression is induced in conditions such as in glucose starvation and viral infection [1,2]. It is homologous to protein disulfide isomerase (PDI) and possesses two thioredoxin domains including an active motif (CGHC) of the disulfide redox response as well as PDI [3]. Recently, it was reported that GRP58 modulates the intracellular signal transduction by interacting with signal transducer and activator of transduction 3 (STAT3) [4], a leptin-related protein, and coexists with cytoplasmic STAT3 and the plasma membrane complexes [5,6]. The aim of this study was determine whether the multiple spots of GRP58-like immunoreactivity were caused by its phosphorylation and how starvation and leptin affected on the patterning of these spots. It was found that serine150 of GRP58 is phosphorylated by fasting and or treatment with leptin.

2. Materials and methods

2.1. Animals and liver sampling

Male Wistar strain rats, weighing 250–300 g, were used. They were housed in a room illuminated for 12 h (lights on 07:00–19:00 h) and kept at 24 ± 1 °C for at least 2 weeks before the experiments. Food (type ME, Oriental Yeast Co., Tokyo) and water were freely available. Animal care and handling were approved by the Institutional Animal Care and Use Committee of Osaka University. Animals were sacrificed by decapitation at 12:00 h [Zeitgeber time (ZT) 5], 18:00 h (ZT11), 24:00 h (ZT17) and 06:00 h (ZT23) and livers were obtained. ZT represents hours after the light turned on under a 12-h light/12-h dark cycle [7].

To determine the effect of fasting, rats were deprived of food and sacrificed at 12, 24, 36 and 48 h after which their livers were harvested and analyzed.

2.2. Two-dimensional gel electrophoresis

Immobilized pH gradient (IPG) gel strips (pH 4–7; NL, 7, 13 and18 cm; Amersham–Pharmacia Biotech) were used as the first dimension gel of 2DE for isoelectric focusing. Liver samples were homogenized in ten volumes of 8 M urea, 60 mM DTT, 2% Chaps, and 10 mM Tris–HCl (pH 7.4), and when examined with protein staining 200 μg of protein was applied on an 18 cm gel strip and examined with mass spectrophotometry. The samples were mixed with 150 μl (for 7 cm gels) or 280 μl (for 13 cm gels) of rehydration buffer containing 7 M urea, 2 M thiourea, 2% Chaps, 10 mM DTT, 2 mM Tris (2-cyanoethyl) phosphine, 2% pharmalyte 3–10, and a trace amount of bromophenol blue, and the gels rehydrated. Isoelectric focusing was then carried out on the gel strips using an electrophoretic apparatus where the voltage was increased stepwise to 4500 V for 18 cm followed by incubation at each voltage for 4–5 h. After the first dimensional electrophoresis, the strips were incubated three times with 5 ml of a solution containing 50 mM Tris–HCl (pH 6.8), 8 M urea, 2% (w/v) SDS, and 60 mM DTT for 30 min, and once with 5 ml of solution containing 50 mM Tris–HCl (pH 6.8), 8 M urea, 2 M thiourea, 20 mM DTT, 30% (w/v) glycerol, 2% (w/v) SDS, and 2 mM Tris(2-cyanoethyl)phosphine for 30 min. In the second dimensional electrophoresis, SDS–polyacrylamide gels (9–16% T/2.6% C) without a stacking gel were used as resolving gels.

2.3. Protein staining and image analysis

After the 2DE, gels were washed for 30 min in a gel fixing solution containing 7% acetic acid and 10% methanol. For maximum sensitivity all gels were stained using SYPRORuby protein gel fluorescent stain

*Corresponding author. Fax: +81 6 6879 8633.
E-mail address: k_nagai@protein.osaka-u.ac.jp (K. Nagai).

Abbreviations: 1DE, one-dimensional electrophoresis; 2DE, two-dimensional electrophoresis; GRP58, glucose-regulated protein 58; PDI, protein disulfide isomerase; STAT, signal transducer and activator of transduction; ZT, zeitgeber time; SDS–PAGE, SDS–polyacrylamide gel electrophoresis; aCSF, artificial cerebrospinal fluid; LCV, lateral cerebral ventricle

0014-5793/$32.00
doi:10.1016/j.febslet.2005.11.074

(BioRad) for 3 h and rinsed in fixing solution for 60 min. Fluorescent signals were detected using a fluorescence image analyzer (Fluorimager 595; Molecular Dynamics).

2.4. 1D-PAGE and 2D-PAGE for Western blotting for analysis of GRP58

For 1D-PAGE, an equal amount of protein from each sample (10 μg) was electrophoresed on an 8% SDS–polyacrylamide gel. For the first dimension of 2D-PAGE, IPG gel strips (pH 4–7; NL, 7 and 13 cm) were used. The sample was mixed with rehydration buffer and applied on a gel (60 μg protein for a 7 cm gel and 100 μg for a 13 cm gel). The voltage for the electrophoresis was increased stepwise to 3000 V at 100 μA intervals for 3–5 h.

After samples were separated by either 1D-PAGE or 2D-PAGE, they were transferred onto a nitrocellulose membrane (Schleicher & Schuell). The membranes were blocked in Tris-buffered saline (pH 7.4) containing 0.1% Tween 20 (Tween-TBS), incubated with rabbit anti-GRP58 polyclonal antibodies (StressGen Biotechnologies) for 3 h, washed with Tween-TBS, incubated with HRP conjugated secondary antibodies (Cell Signaling Technology) against rabbit IgG for 1 h, and washed with Tween-TBS. Immunoreactivity to the anti-GRP58 antibodies was visualized using an enhanced chemiluminescence system (NEN Life Science Products).

2.5. MALDI-TOF-mass spectrometry

Gel sections from the 2-DE gels were incubated with 1 ml of 50 mM ammonium bicarbonate-50% methanol at 37 °C overnight. The solution was then removed and the gel sections incubated in a solution containing 100 μl of 10 mM DTT-100 mM ammonium bicarbonate for 60 min at 60 °C. The gels were alkylated with 100 μl of 50 mM iodoacetamide/50 mM ammonium bicarbonate for 30 min at room temperature. The gels were washed twice with distilled water and dried under a vacuum pump. The gels were then digested with 50 μl of 50 mM ammonium bicarbonate containing 10% acetonitrile and 1 pmol of trypsin (Sigma) for 16 h at 37 °C and resultant peptides eluted in a solution containing 50% acetonitrile, 50 mM ammonium bicarbonate, and 0.1% TFA. The supernatant obtained after centrifugation was concentrated to a volume below 30 μl under vacuum and desalted with ZipTip 18 (Millipore). For measurement of mass spectrometry (MS) spectra, 0.5 μl of sample solution was mixed with 0.5 μl of matrix solution containing 10 mg/ml α-cyano-4-hydroxycinnamic acid (CHCA), deposited on the target, and dried completely. MALDI-TOF-mass spectra were generated using an AXIMA-CFR instrument (Shimadzu Corp., Japan) under reflectron mode operating conditions after calibration using ACTH and bradykinin. Peptides were matched using the MASCOT database search under the following conditions: fixed modifications of carbamidomethyl (C); variable modifications of phosphorylated Ser and Thr; Taxonomy of Rattus; and a tolerance of one missed cleavage.

2.6. Alkaline phosphatase treatment

Sample was incubated with 0.5 μl alkaline phosphatase (New England BioLab) for 12 h at 4 °C. Then the sample was separated with SDS–PAGE, and immunoblotted using anti-GRP58 antibodies.

2.7. Leptin injection

For intracranial administration of leptin, a brain cannula, made of PE-10 (Clay Adams, Parsippany, NJ), was inserted into the right lateral cerebral ventricle (LCV), three days before the experiment under pentobarbital anesthesia (35 mg/kg) as previously described [8]. The effect of leptin on GRP58 was examined by injecting leptin [Sigma–Aldrich, 10 μg/20 μl of artificial cerebrospinal fluid (aCSF)] into the LCV at each time point under unanesthetic condition using the LCV cannula. For control experiment, 20 μl of aCSF was injected into the LCV. Animals were sacrificed at 0, 15, 30, 60, and 180 min after the administration of leptin or aCSF and liver samples were obtained.

2.8. Anti-phosphorylated GRP58 Ser-150 antibody production

A synthetic peptide, EFKKFIpSDKDASC (corresponding to amino acid residues of GRP58 surrounding Ser150) was conjugated with Imject Maleimide activated mcKLH (Pierce), mixed with Freund's complete adjuvant and injected into rabbits. The resultant polyclonal antiserum against this peptide was subjected to affinity purification and used to detect GRP58 phosphorylated on Ser150.

2.9. Dephosphorylation of proteins using hydrogen fluoride–pyridine

Dephosphorylation of proteins using hydrogen fluoride–pyridine was performed as described previously [9]. Samples were dephosphorylated using hydrogen fluoride–pyridine, neutralized with NaOH, desalinated by using a centrifugal filter (Millipore), then eluted in TNE buffer.

2.10. Immunoprecipitations

Protein samples were pre-treated with protein G–Sepharose (Amersham-Pharmacia Biotech) for 1 h at 4 °C. After centrifugation, the supernatant was incubated for 1 h at 4 °C with protein G–Sepharose that had been preincubated with 2 μg of mouse anti-Stat3 antibody (BD Biosciences Pharmingen) or mouse IgG. The Sepharose beads were washed five times with TNE buffer. Immunoprecipitated proteins were analyzed using SDS–PAGE electrophoresis.

3. Results

3.1. GRP58 identified as a protein showing daily changes in its expression in rat liver

To identify proteins showing daily changes in their expression in the rat liver, livers were sampled at 18:00 h (ZT11) and 06:00 h (ZT23) and their proteins were separated by 2DE after homogenization. The 2DE-gels were stained with SYPRO Ruby and about 1200 spots were detected in gels of pH 4–7 after a comparative analysis of the protein patterns was carried out using the image analysis software, PDQUEST. Among the proteins that showed changes in their expression patterns, a spot (shown as arrow heads in Fig. 1A) was identified that appeared to undergo daily changes in its expression pattern (high at ZT11 and low at ZT23) after quantitative analysis. Peptide mass fingerprinting of 21 fragments generated from the spot showed that they matched the amino acid sequence of GRP58 with a MASCOT score of 243, and a sequence coverage of 39%, indicating that this protein is GRP58 (Table 1).

3.2. Confirmation of the protein as GRP58

To confirm that the above protein spot is actually GRP58, livers were sampled at ZT 5, 11, 17, and 23, examined by SDS–PAGE and immunoblotted using a rabbit anti-GRP58 polyclonal antibodies. However, a clear daily change in the immunoreactivity to the anti-GRP58 antibodies was not detected in 1DE (Fig. 1B), even though a clear shift in the migration of the immunoreactive band was observed at ZT11 in comparison with sample bands obtained at other time points (Fig. 1B). These results suggested that this protein might undergo protein modification such as phosphorylation. The protein was examined further using 2DE and immunoblotting with the anti-GRP58 antibodies which detected four immunoreactive spots of similar molecular sizes but with different isoelectric points (1-1, 1-2, 1-3 and 1-4 in Fig. 1C). The spot identified in Fig. 1A (arrowheads) was identical to the spot at 1-3 in Fig. 1C. Immunoreactivities of the GRP58-like immunoreactive substance (GRP58LIS) at more acidic isoelectric points (1-3 and 1-4) increased at ZT11 in comparison to those at other time points (Fig. 1C).

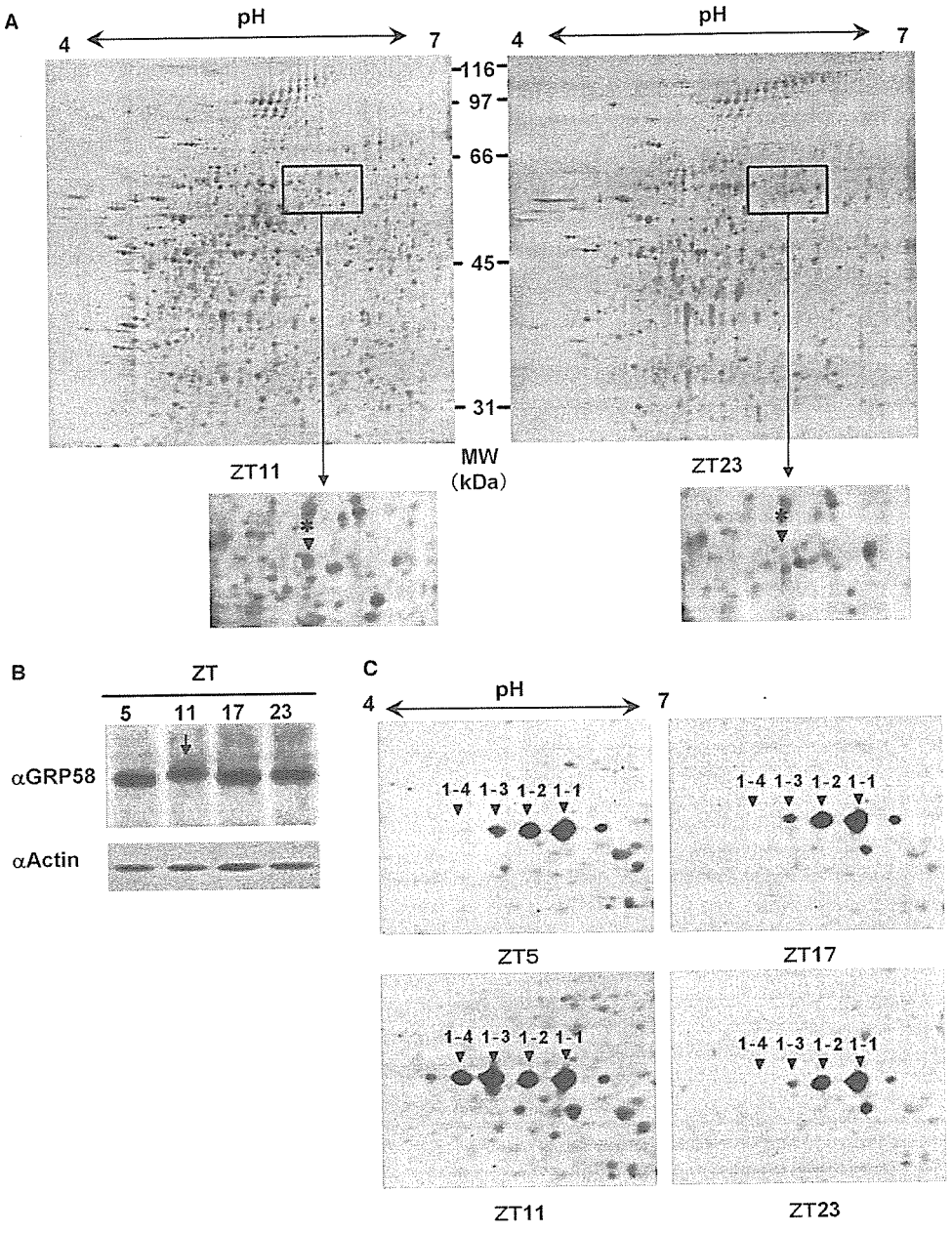

Fig. 1. Detections of proteins exhibiting daily expression changes in the liver. (A) 2DE of rat liver was sampled at ZT11 and ZT23 with isoelectric focusing showed different expression patterns for spot showed by arrowheads. (B) Immunoblotting using an anti-GRP58 antibody in 1DE. Livers were sampled at 12:00 (ZT5), 18:00 (ZT11), 24:00 (ZT17) and 06:00 (ZT23) h under 12-h light and 12-h dark period (light on at 07:00 h). Livers were homogenized, centrifuged, and supernatants were dissolved in SDS–PAGE sample buffer. Samples then underwent electrophoresis and were immunoblotted using anti-GRP58 antibodies. (C) Immunoblotting using an anti-GRP58 antibodies in 2DE. Different expression patterns were observed spots 1-1, 1-2, 1-3 and 1-4.

3.3. Phosphorylation of GRP58

Since horizontal movement of the protein spots in the 2DE is often observed due to changes in isoelectric point induced by protein phosphorylation, the result obtained in the experiment shown in Fig. 1C raised the possibility that phosphorylation of GRP58 might be increased at ZT11. To examine whether GRP58 was phosphorylated at ZT11, the liver sample obtained at ZT11 was treated with alkaline phosphatase and examined by immunoblotting. As seen in Fig. 2, after treatment with phosphatase, the mobility of GRP58LIS at ZT11 slightly increased in 1DE (Fig. 2A) and the immunoreactivities of 2 spots in the more acidic side (1-3 and 1-4) decreased while the immunoreactivity of the spot at the most alkaline side (1-1) increased at ZT11 in 2DE gel (Fig. 2B). These findings suggest that GRP58 is phosphorylated at ZT11.

3.4. Effects of fasting

Since protein expression in the liver is known to be frequently affected by fasting and ZT11 is almost at the end of the resting (non-eating) period for nocturnal animals like rats, it was hypothesized that the above daily change in GRP58 mobility might be affected by fasting. Therefore, liver samples

Table 1
Mascot search results for fragments of protein spots corresponding to GRP58

Signal	Observed	Mr(expt)	Mr(calc)	Delta	Miss	Start-end	Sequence	Spot no.			
1	1191.70	1190.69	1190.59	0.10	0	63–73	LAPEYEAAATR	1-1	1-2	1-3	1-4
2	1397.81	1396.80	1396.57	0.23	0	83–94	VDCTAVTNTCNK	1-1	1-2	1-3	1-4
3	1652.88	1651.87	1651.76	0.11	1	105–119	IFRDGEEAGAYDGPR	1-1	1-2	1-3	1-4
4	817.48	816.47	816.38	0.09	1	147–152	KFIpSDK			1-3	1-4
5	1587.91	1586.90	1586.81	0.09	1	148–161	FISDKDASVVGFFR	1-1	1-2		
6	1394.75	1393.74	1393.65	0.09	0	162–173	DLFSDGHSEFLK	1-1	1-2	1-3	
7	1607.83	1606.82	1606.74	0.08	0	259–271	DLLTAYYDVDYEK	1-1	1-2	1-3	1-4
8	1951.01	1950.00	1949.93	0.08	1	259–274	DLLTAYYDVDYEKNTK			1-3	
9	782.38	781.37	781.35	0.02	0	275–280	GSNYWR	1-1	1-2	1-3	1-4
10	1747.05	1746.04	1745.92	0.12	1	289–304	TFLDAGHKLNFAVASR	1-1	1-2	1-3	1-4
11	877.52	876.51	876.48	0.03	0	297–304	LNFAVASR	1-1	1-2	1-3	1-4
12	2733.30	2732.29	2732.40	−0.11	1	305–329	KTFSHELSDFGLESTTGEIPVVAIR	1-1	1-2	1-3	1-4
13	2605.24	2604.23	2604.31	−0.07	0	306–329	TFSHELSDFGLESTTGEIPWAIR	1-1	1-2	1-3	1-4
14	1172.61	1171.60	1171.53	0.07	0	336–344	FVMQEEFSR	1-1	1-2	1-3	1-4
15	1472.78	1471.77	1471.68	0.10	1	336–347	FVMQEEFSRDGK	1-1	1-2	1-3	
16	1529.89	1528.88	1528.77	0.12	1	352–363	FLQEYFDGNLKR	1 -1	1-2	1-3	1-4
17	1801.03	1800.02	1799.93	0.09	1	364–379	YLKSEPIPETNEGPVK			1-3	
18	1341.74	1340.73	1340.68	0.06	0	449–460	GFPTIYFSPANK	1-1	1-2	1-3	1-4
19	1469.86	1468.85	1468.77	0.08	1	449–461	GFPTIYFSPANKK	1-1	1-2	1-3	1-4
20	1363.76	1362.75	1362.71	0.04	0	472–482	ELNDLISYLQR				
21	1593.92	1592.91	1592.84	0.07	0	483–496	EATNPPIIQEEKPK	1-1	1-2	1-3	

MALDI-TOF-mass spectra were obtained using an AXIMA-CFR instrument (Shimadzu Corp., Japan). The MASCOT data base search identified Spot1-3 as a glucose-regulated protein of 58 kDa. Twenty-one peaks were matched to GRP58 with a score of 243 and a sequence coverage of 39%. The following conditions were used for searching the database: fixed modifications of carbamidomethyl (C); variable modifications included phosphorylated Ser and Thr; Taxonomy: Rattus; peptide tolerance: ±0.3 Da (Table 1).
Mr(expt), expected molecular mass; Mr(calc), calculated molecular mass.

were obtained from rats at 0 h and after 12, 24, 36 and 48 h of food deprivation. Mobility of GRP58LIS on 1DE gel was decreased when the liver samples were obtained after 12- and 24-h fasting in comparison to those obtained at the other time points (Fig. 2C). When these samples were analyzed on 2DE gels, it was observed that after 12- and 24-h fasting, the immunoreactivities of GRP58LIS at more acidic side (1-3 and 1-4 in Fig. 2D) were elevated but that those at 36- and 48-h of fasting were decreased (Fig. 2D). These findings indicate that phosphorylation of GRP58 in the liver is induced by fasting.

3.5. Effect of intracranial injection of leptin

Recently, it was suggested that GRP58 interacts with STAT3 to modulate intracellular signal transduction [4–6]. Since STAT3 was suggested to be involved in the intracellular signal transduction of leptin and a functional leptin receptor exists in the brain [10], the effect of intracranial injection of leptin on the mobility of GRP58 was examined. Three hours after leptin (Sigma–Aldrich, 10 μg/20 μl of a CSF) was injected into LCV using the LCV cannulae under un-anesthetic condition, the mobility of GRP58LIS from the liver was clearly shifted in 1DE (Fig. 2E) and the immunoreactivities of GRP58LIS with acidic isoelectric points (1-3 and 1-4 in Fig. 2D) increased in 2DE.

3.6. Phosphorylation site of GRP58 induced by fasting and leptin

To identify the phosphorylation site(s) of GRP58 after 12-h fasting, peptide mass finger printing was carried out on the four spots of GRP58LIS (1-1, 1-2, 1-3, 1-4 in Fig. 2D). The mass spectrometry data showed that a fragment of 1587.91 Da (sequence of GRP58 between amino acids (aa) 148–161; FISDKDASVVGFFR in Table 1) was present in spots 1-1 and 1-2 but not in spots 1-3 and 1-4. Since phosphorylated fragment was sometimes hardly detected with MALDI-TOF-MS, it was possible that this fragment was phosphorylated in spots 1-3 and 1-4. Furthermore, the molecular mass of the first half fragment (corresponding to KFISDK) was 80 Da higher than that of the calculated molecular mass of the fragment, indicating that it was phosphorylated on one of the internal serine residues, most probably serine 150. It was also possible that unphosphorylated KFISDK (736 Da) might not be detected because of the lower mass than detecting threshold MALDI-TOF-MS. In order to obtain further support for the phosphorylation of this residue after fasting and leptin injection, we conducted a search using NetPhos which allows sequence- and structure-based prediction of eukaryotic protein phosphorylation sites [11]. NetPhos predicted with strong probability that the serine residue at aa 150 of GRP58 would be phosphorylated. To test this possibility, a rabbit polyclonal antibodies against the sequence from 144 to 156 of phosphorylated GRP58 (EFKKFIpSDKDASC)-conjugated with KLH was generated. This anti-phosphoGRP58 antibody was first used to examine the phosphorylation states of Ser-150 in the liver after 12-h fasting. Fasting for 12 h induced a band shift of GRP58LIS (Fig. 3Aa) and increased the immunoreactivity of a band migrating at 60 kDa to anti-phosphoGRP58 antibody in 1DE (Fig. 3Ab). Furthermore, when anti-phosphoGRP58 antibody was preabsorbed with the antigen (EFKKFIpSDKDASC), immunoreactivity to the anti-phosphoGRP58 antibody disappeared in 1DE (Fig. 3Ac). Immunoreactivity to this anti-phosphoGRP58 antibody was observed only in the spots corresponding to 1-3 and 1-4 in 2DE (Fig. 3B). In controls, anti-phosphoGRP58 was preabsorbed to the antigen (EFKKFIpSDKDASC), which eliminated all immunoreactivity to anti-phosphoGRP58 in 2DE (data not shown). Three hours after interacranial injection of leptin immunoreactivity to anti-phosphoGRP58 increased in both 1DE or 2DE (spots 1-3 and 1-4) (data not shown). These observations indicate that 12-h fasting

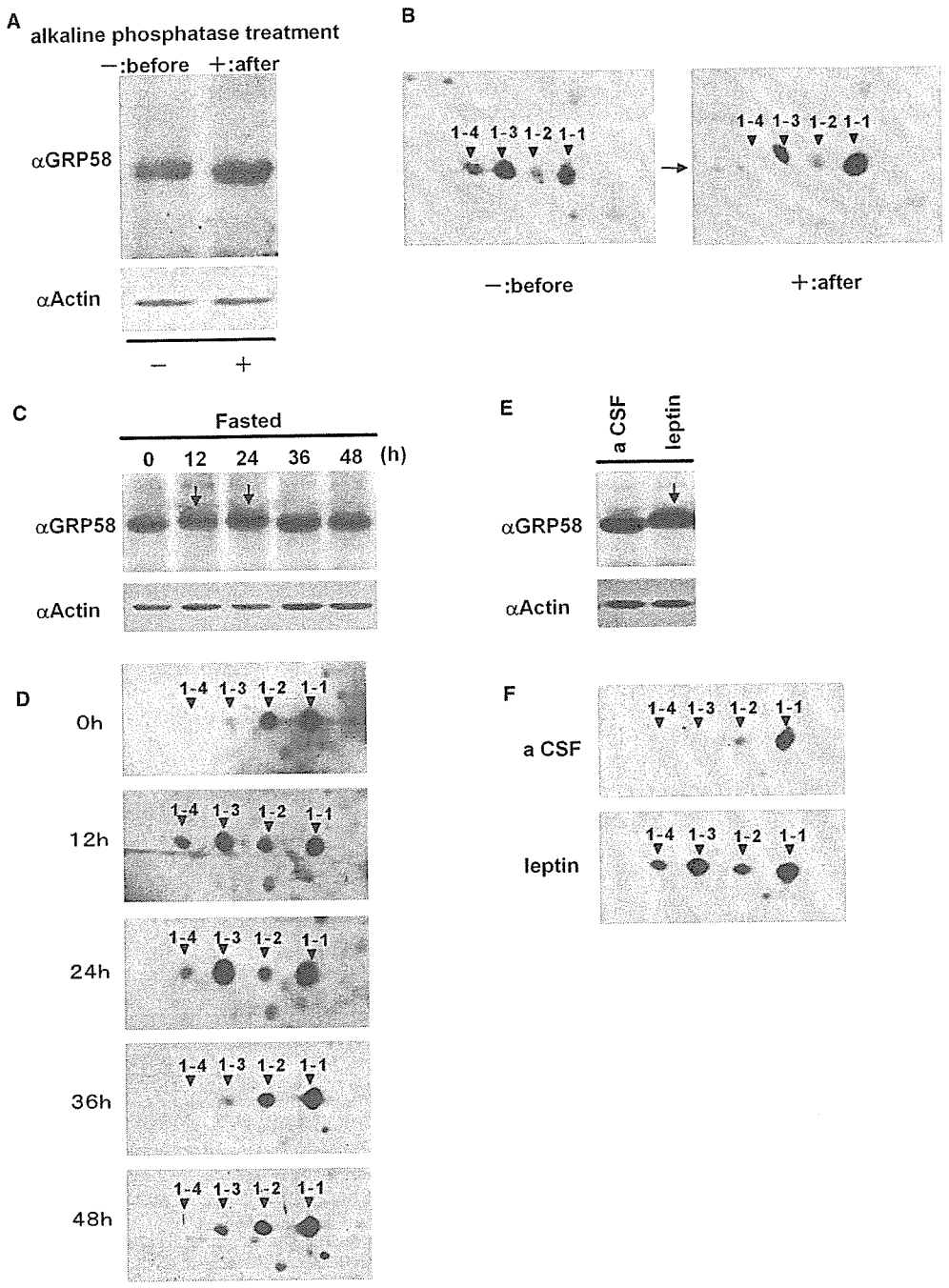

Fig. 2. Mobility changes in 1DE (A) and 2DE (B) after phosphatase treatment (A, B), fasting (C, D), and leptin injection (E, F). (A, B) Liver samples were obtained from rats at ZT11 and immunoblot analyses were carried out using anti-GRP58 antibodies before and after treatment with alkaline phosphatase in 1DE (A) and 2DE (B). (C, D) Effect of fasting on GRPLIS. Livers were obtained from rats at 0, 12, 24, 36 and 48 h after the start of food deprivation, homogenized and loaded onto 1DE and 2DE gels. After electrophoresis, immunoblot analyses were performed using an anti-GRP58 antibodies in 1DE (C) and 2DE (D). (E, F) Effect of leptin on GRP58LIS. Liver samples were obtained 3 h after the administration of leptin or aCSF and immunoblot analyses performed using an anti-GRP58 antibodies in 1DE (E) and 2DE (F).

and intracranial injection of leptin elevate phosphorylation of Ser-150 of GRP58.

To examine the possible role of GRP58 phosphorylation at aa 150 in intracellular signal transduction, an immunoprecipitation study was carried out using mouse anti-STAT3 monoclonal antibody. In an control experiment, it was observed that GRP58 was not precipitated with an anti-BIT (brain immunoglobulin-like molecule with tyrosine-based activation motifs) monoclonal antibody; 1D4, which is kindly given by Dr. Shin-ichiro Sano (Mitsubishi Kasei Industitute of Life Sciences, Japan) [12]. Therefore, above observation seems to be specific.

In this experiment, liver samples were obtained 3 h after the intracranial injection of leptin or aCSF and immunoreactivities to anti-GRP58 and anti-phosphoGRP58 antibodies were examined. As seen in Fig. 3C, immunoprecipitation using anti-STAT3 antibody precipitated GRP58LIS in the livers of rats injected with either leptin or aCSF. However, the immu-

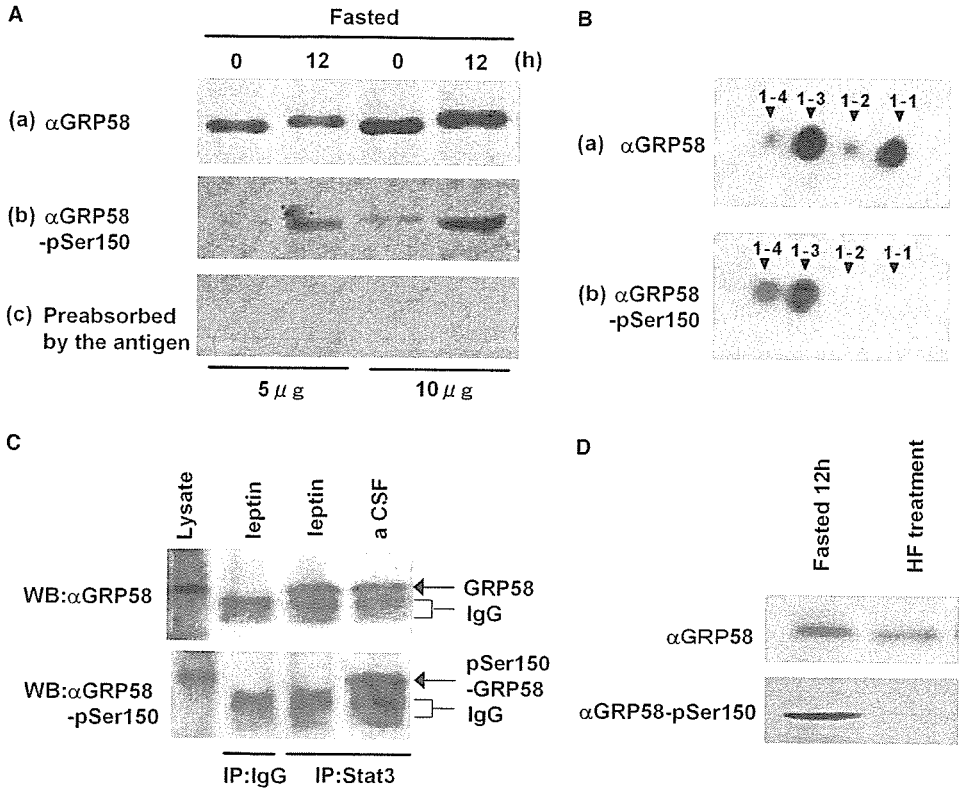

Fig. 3. Changes in immunoreactivity to anti-phosphoGRP58 antibody due to fasting and intracranial injection of leptin. (A, B) Immunoblot analyses of liver samples obtained at 0 and 12 h fasting using an anti-GRP58 and anti-phosphoGRP58 antibodies in 1DE (A) and 2DE (B). Specificity of the anti-phosphoGRP58 antibody was confirmed by preabsorbing it with the antigen. (C) Immunoprecipitation studies using anti-STAT3 antibody and IgG. Liver samples were obtained from rats 3 h after injections of leptin and aCSF and analyzed via immunoblotting. (D) Effect of dephosphorylation of GRP58 using hydrogen fluoride–pyridine on anti-GRP58 and anti-phosphoGRP58 immunoreactivity in livers obtained after 12-h fasting.

noreactivity to anti-phopshoGRP58 was immunoprecipitated by the anti-STAT3 antibody in the liver of aCSF-injected rats but not in that of leptin-injected rats, which indicates that the GRP58 phosphorylated at serine 150 is not able to bind STAT3.

To confirm the phosphorylation of GRP58 after fasting for 12 h, the effect of a dephosphorylation treatment using 70% hydrogen fluoride–pyridine on the immunoreactivity to anti-phosphoGRP58 antibodies in rats was examined. As seen in Fig. 3D, the immunoreactivity to the anti-phosphoGRP58 observed in rats fated for 12 h, disappeared following treatment with hydrogen fluoride–pyridine. This observation also confirms that GRP58 is phosphorylated at aa 150 after fasting.

4. Discussion

In this study, proteins showing daily changes in their rat liver expression patterns were identified via proteome analysis using 2DE and mass spectrometry. As a result, time-dependent changes in protein spots were detected with GRP58 being identified as one of the protein spots showing daily changes (Fig. 1; Table 1). GRP58 is a stress protein that is localized in the lumen of the endoplasmic reticulum because the C-terminus has an ER-retention signal. It is thought to be important for disulfide bond formation of proteins in the endoplasmic reticulum [13–15]. Recent data confirms the association between GRP58 and STAT3 in cytosolic statsome I complexes and indicates that both GRP58 and STAT family members co-associate in the plasma membrane compartment [4]. Thus, it is speculated that GRP58 might regulate signal transduction by sequestering active and inactive STAT3.

Therefore, it was of interest to characterize the daily changes in GRP58 expression in the rat liver. Although no daily change in the amount of GRP58LIS was observed, a shift in its mobility was observed at ZT11 in 1DE (Fig. 1B). Four GRP58LIS spots with similar molecular sizes but with different isoelectric points were observed in a time-dependent manner by immunoblotting in 2DE (Fig. 1C). Since horizontal scattering of spots in 2DE derived from the same protein with similar molecular weight is often the result of protein phosphorylation, it was hypothesized that GRP58 in the rat liver might be time-dependently phosphorylated in a time-dependent manner. This hypothesis was tested by examining the effect of an alkaline phosphatase on the migration of GRP58LIS obtained from liver samples at ZT11 in 1DE and 2DE. The phosphatase treatment slightly increased the mobility of GRP58LIS in 1DE (Fig. 2A) and reduced the immunoreactivities of the two GRP58LIS spots on the more acidic side (1-3 and 1-4) while enhancing the immunoreactivity of the spot on the most alkaline side (1-1) in 2DE gel (Fig. 2B). Altogether, these findings suggest that GRP58 is phosphorylated at ZT11.

Since ZT11 is almost at the end of the light period, it was possible that the mobility changes of GRP58 in 1DE and 2DE might be caused by food deprivation. This idea is supported by a recent report showing changes in the mobility of

ERp57 (GRP58) during recovery from ATP depletion using a cell culture based reversible ATP depletion model [16]. Therefore, the effect of food deprivation on the mobility of GRP58 was examined. As seen in Fig. 2C and D, food deprivation for 12 and 24 h caused a shift in the mobility of GRP58LIS in 1DE and increased the immunoreactivity of GRP58LIS on the acidic side (1-3 and 1-4 in Fig. 2D) in 2DE. These results indicate that GRP58 is phosphorylated after 12- and 24-h fasting. Glycogenolysis and gluconeogenesis in the liver are induced at ZT11 and after certain periods of fasting. Thus, the phosphorylation of GRP58 might be related to the mechanism of these processes.

As mentioned above, GRP58 is known to interact with STAT3 [4] and is thought to be involved in the intracellular signal transduction of leptin. As leptin might induce phosphorylation of GRP58, the effect of intracranial injection of leptin on the mobility of GRP58LIS in 1DE and 2DE was examined. Leptin induced a mobility shift of GRP58LIS in 1DE (Fig. 2E) and increased the immunoreactivities of GRP58LIS on the more acidic side in 2DE (1-3 and 1-4 in Fig. 2F), suggesting that GRP58 phosphorylation is induced by leptin.

Phosphorylation of GRP58 was found to occur at Ser150 after 12-h fasting and leptin injection. Moreover, it was found that dephosphorylation of GRP58 using hydrogen fluoride–pyridine eliminated immunoreactivity to anti-phosphoGRP58 antibody in liver samples obtained from rats fasted for 12 h (Fig. 3D). This observation confirmed that fasting induces phosphorylation of GRP58.

Immunoprecipitation using anti-STAT3 antibody (Fig. 3C) indicated that phosphorylation of GRP58 at Ser150 renders in unable to bind to STAT3. Since it has been suggested that GRP58 and STAT3 co-associate in the plasma membrane compartment [4], it is possible that unphosphorylated, but not phosphorylated GRP58 binds to STAT3. Thus, phosphorylation of GRP58 at Ser150 may constitute the signal that frees STAT3 from the plasma membrane compartment, resulting in the activation of the downstream signal transduction pathway. In this respect, it was found that GRP58 is present in STAT3-DNA complexes within the nucleus and is a necessary component them [17], suggesting that GRP58 is related to the nuclear entry and transcriptional regulation of STAT3.

In the current report, it is known that GRP58 of rat spleen is phosphorylated in three tyrosines (Y 444, Y 453 and Y466) by the Src-like tyrosine kinase Lyn [18]. Therefore, it is possible that spots of 1-1 and 1-2 may represent different phosphorylation states of these tyrosine residues.

These possibilities will be examined in future studies together with analyses of the constituents of spots 1-1 and 1-2, and of kinase responsible for the phosphorylation of aa 150 of GRP58.

References

[1] Lee, A.S. (1987) Coordinated regulation of a set of genes by glucose and calcium ionophores in mammalian cells. Trends Biochem. Sci. 12, 20–23.

[2] Mazzarella, R.A., Marcus, N., Haugejorden, S.M., Balcarek, J.M., Baldassare, J., Roy, B., Li, L.J., Lee, A.S. and Green, M. (1994) Erp61 is GRP58, a stress-inducible luminal endoplasmic reticulum protein, but is devoid of phosphatidylinositide-specific phospholipase C activity. Arch. Biochem. Biophys. 308, 454–460.

[3] Hirano, N., Shibasaki, F., Sakai, R., Tanaka, T., Nishida, J., Yazaki, Y., Takenawa, T. and Hirai, H. (1995) Molecular cloning of the human glucose-regulated protein ERp57/GRP58, a thiol-dependent reductase. Identification of its secretory form and inducible expression by oncogenic transformation. Eur. J. Biochem. 234, 336–342.

[4] Guo, G.G., Patel, K., Kumar, V., Shah, M., Fried, V.A., Etlinger, J.D. and Sehgal, P.B. (2002) Association of the chaperone glucose-regulated protein 58 (GRP58/ER-60/ERp57) with Stat3 in cytosol and plasma membrane complexes. J. Interferon Cytokine Res. 22, 555–563.

[5] Ndubuisi, M.I., Guo, G.G., Fried, V.A., Etlinger, J.D. and Sehgal, P.B. (1999) Cellular physiology of STAT3: Where's the cytoplasmic monomer?. J. Biol. Chem. 274, 25499–25509.

[6] Sehgal, P.B., Guo, G.G., Shah, M., Kumar, V. and Patel, K. (2002) Cytokine signaling: STATS in plasma membrane rafts. J. Biol. Chem. 277, 12067–12074.

[7] Schibler, U. (2003) Liver regeneration clocks on. Science 302, 234–235.

[8] Chun, S., Niijima, A., Nagai, N. and Nagai, K. (1998) Effect of bilateral lesions of the suprachiasmatic nucleus on hyperglycemia caused by 2-deoxy-D-glucose and vasoactive intestinal peptide in rats. Brain Res. 809, 165–174.

[9] Kuyama, H., Toda, C., Watanabe, M., Tanaka, K. and Nishimura, O. (2003) An efficient chemical method for dephosphorylation of phosphopeptides. Rapid Commun. Mass Spectrom. 17, 1493–1496.

[10] Schwartz, M.W., Woods, S.C., Porte Jr., D., Seeley, R.J. and Baskin, D.G. (2000) Central nervous system control of food intake. Nature 404, 661–671.

[11] Blom, N., Gammeltoft, S. and Brunak, S. (1999) Sequence and structure-based prediction of eukaryotic protein phosphorylation sites. J. Mol. Biol. 294 (5), 1351–1362.

[12] Sano, S., Matsuda, Y. and Nakagawa, H. (1989) A novel brain-specific antigen: a glycoprotein electrophoretically similar to but immunochemically different from type B nucleoside diphosphatase. J. Biochem. 105, 457–460.

[13] Murthy, M.S. and Pande, S.V. (1994) A stress-regulated protein. GRP58, a member of thioredoxin superfamily, is a carnitine palmitoyltransferase isoenzyme. Biochem. J. 304, 31–34.

[14] Koivunen, P., Horelli-Kuitunen, N., Helaakoski, T., Karvonen, P., Jaakkola, M., Palotie, A. and Kivirikko, K.I. (1997) Structures of the human gene for the protein disulfide isomerase-related polypeptide ERp60 and processed gene and assignment of these genes to 15q15 and 1q21. Genomics 42, 397–404.

[15] Lindquist, J.A., Jensen, O.N., Mann, M. and Hammerling, G.J. (1998) ER-60, a chaperone with thiol-dependent reductase activity involved in MHC class I assembly. EMBO J. 17, 2186–2195.

[16] Kumar, Y. and Tatu, U. (2003) Stress protein flux during recovery from simulated ischemia: induced heat shock protein 70 confers cytoprotection by suppressing JNK activation and inhibiting apoptotic cell death. Proteomics 3, 513–526.

[17] Margherita, E., Sabina, C., Fabio, A., Caterina, G., Anna, F. and Carlo, T. (2004) ERp57 is present in STAT3-DNA complexes. Biochem. Biophys. Res. Commun. 323, 1306–1312.

[18] Donella-Deana, A., James, P., Staudenmann, W., Cesaro, L., Marin, O., Brunati, A.M., Ruzzene, M. and Pinna, L.A. (1996) Isolation from spleen of a 57-kDa protein substrate of the tyrosine kinase Lyn. Identification as a protein related to protein disulfide-isomerase and localization of the phosphorylation sites. Eur. J. Biochem. 235, 18–25.

Available online at www.sciencedirect.com
ScienceDirect
Biochemical and Biophysical Research Communications 352 (2007) 579–586
BBRC
www.elsevier.com/locate/ybbrc

Evaluation of laser microdissection as a tool in cancer glycomic studies

Hiroaki Korekane [a,b], Kyoko Shida [a,b], Kohei Murata [c], Masayuki Ohue [c], Yo Sasaki [c], Shingi Imaoka [c], Yasuhide Miyamoto [a,*]

[a] *Department of Immunology, Osaka Medical Center for Cancer and Cardiovascular Diseases, 1-3-2 Nakamichi, Higashinari-ku, Osaka 537-8511, Japan*
[b] *Japan Health Sciences Foundation, 13-4 Nihonbashi Kodenma-cho, Chuo-ku, Tokyo 103-0001, Japan*
[c] *Department of Surgery, Osaka Medical Center for Cancer and Cardiovascular Diseases, 1-3-3 Nakamichi, Higashinari-ku, Osaka 537-8511, Japan*

Received 18 October 2006
Available online 14 November 2006

Abstract

Laser microdissection (LMD) is a recent development that enables the isolation of specific cell populations from tissue sections. This study focuses on the potential of LMD as a tool in cancer glycomics using colon cancer as a model. LMD was performed on hematoxylin and eosin stained frozen tissue sections. Tumor cells and normal epithelial cells were selectively microdissected. *N*-Glycans from the LMD- and the bulk tissue-derived samples were liberated by hydrazinolysis and then labeled with 2-aminopyridine. After sialidase digestion, the resulting asialo-*N*-glycans were analyzed by normal and reversed phase HPLC combined with mass spectrometry. Comparison of the various *N*-glycan profiles with the aid of LMD identified seven characteristic *N*-glycans with significantly different expression profiles between normal and cancerous cells that could not be detected by conventional analysis. Thus, LMD is a potent and useful tool for analyzing variations in the expression of *N*-glycans by overcoming the problem of tissue sample heterogeneity.

Keywords: Colon cancer; Glycomics; Microdissection; *N*-Glycans; Pyridylamination

It is well known that glycans on the cell surface or in the extracellular space play important roles in cellular differentiation, adhesion, and proliferation [1,2]. The biosynthesis of glycans is tissue-specific and is regulated not only by physiological conditions, but also by pathological conditions such as tumorgenesis [3–5]. Aberrant glycosylation of membrane components occurs in essentially all types of human cancers, and many glycosyl epitopes constitute tumor-associated carbohydrate antigens (TACAs) [6–8]. Many lines of evidence suggest that the TACAs function mainly as adhesion molecules and contribute to cancer metastasis [7,9–11]. Alteration of the expression profile of TACAs in certain types of cancer has prompted researchers to evaluate their potential use as diagnostic and/or prognostic tools.

The application of glycomics to cancer research can highlight changes in the expression profile of the glycans occurring during tumor development and progression, leading to the identification of new molecular markers or potential therapeutic targets. However, because cancer tissue is composed of multiple subpopulations of cells, including normal epithelial cells, stromal cells, inflammatory cells, and angiogenic elements, accurate molecular analysis requires isolation of the tumor cells. Laser microdissection (LMD) is a recently developed technique that permits the reliable procurement of specific cell populations from tissue sections under direct microscopic observation. The laser-assisted microdissection technique has already been extensively used to isolate specific types of cells for the molecular analysis of DNA, RNA, and protein. However, in the field of glycan research, only one application of this technique for the analysis of glycosaminoglycans in postmortem human LASIK corneas has been reported [12]. Because LMD is a highly time consuming technique, feasibility

* Corresponding author. Fax: +81 6 6972 7749.
E-mail address: miyamoto-ya@mc.pref.osaka.jp (Y. Miyamoto).

0006-291X/$ - see front matter © 2006 Elsevier Inc. All rights reserved.
doi:10.1016/j.bbrc.2006.10.191

and usefulness of this procedure must be thoroughly evaluated prior to its application in the analysis of glycans in cancer specimens.

In this study, we have investigated the potential of LMD as a tool in cancer glycomic studies using colon cancer as a model. Asialo-PA-*N*-glycans were prepared from bulk colon cancer tissue, bulk normal colon tissue, and from both normal colonic epithelial cells and cancerous colonic cells isolated from the bulk tissue using LMD. The *N*-glycans were then analyzed by normal and reversed phase HPLC in combination with mass spectrometry. LMD enabled us to identify seven characteristic *N*-glycans which displayed remarkable differences in the expression profile between normal and cancerous colon cells that could not be detected by conventional techniques. Our results demonstrate the usefulness of LMD for the accurate analysis of *N*-glycans in cancer glycomic studies.

Materials and methods

Standard PA-oligosaccharides. The structures and abbreviations of the authentic PA-oligosaccharides used in this study are listed in Table 1. Authentic PA-sugars were obtained from the following suppliers: 224F from Takara (Shiga, Japan); 22bis, ag22bisF, $G_1$22bisF, and 22bisF from Seikagaku Co. (Tokyo, Japan). Ag22bis was prepared by digestion of 22bis with Jack bean β-galactosidase (Seikagaku Co.). The structure of ag22bis was verified by normal and reversed phase HPLC analyses, combined with successive exoglycosidase digestions and by mass spectrometric analysis.

Tissue. Paired samples of normal and cancerous colon were obtained from the same patient by a standard colectomy procedure. Areas of tissues examined were selected by an experienced gastrointestinal pathologist. The tissue was cut into blocks, embedded in OCT compound (Sakura Finetechnical, Tokyo, Japan), snap frozen in liquid nitrogen, and stored at −80 °C until use. This study was approved by Local Ethics Committee of Osaka Medical Center for Cancer and Cardiovascular Diseases. Informed consent was obtained from the patient.

Laser microdissection. Frozen tissue sections (8 μm thick) of either cancerous colon or normal colonic mucosa were cut on a cryostat, CM 1900 microtome (Leica, Milton Keynes, UK). Tissue sections were thaw mounted on to a film-coated glass slide (90FOIL-SL25, Leica), briefly air dried, and then fixed at room temperature in 95% ethanol for 1 min. Staining was performed by the following procedure. Sections were immersed in Mayer's hematoxylin solution (Muto Pure Chemicals, Tokyo, Japan) for 30 s at room temperature, washed with phosphate-buffered saline (PBS) until a vivid blue color appeared, and then immersed in pure eosin solution (Muto Pure Chemicals) for 2 s. The sections were then dehydrated in 100% ethanol for 30 s and air dried. Laser microdissection (LMD) was performed using a Leica AS LMD system.

Preparation of protein extracts. After microdissection, the microdissected cells were carefully transferred from a PCR tube to a glass centrifuge tube using water and a micropipette. The collected cells were lyophilized and then solubilized in a 1:1 mixture of hexafluoroisopropanol (HFIP) [13,14] and 0.2% acetic acid. Control samples, which had not been subjected to LMD, were prepared from the frozen tissue sections cut directly into the solubilization mixture. The protein concentration was determined with a BCA protein assay kit (Pierce, Rockford, IL) using bovine serum albumin as a standard. A protein sample of 300 μg was collected, concentrated, and used for the preparation of PA-*N*-glycans.

Preparation of PA-N-glycans. *N*-Glycans were liberated from the glycoproteins by hydrazinolysis at 100 °C for 10 h and then re-*N*-acetylated with acetic anhydride in a saturated sodium bicarbonate solution as previously described [15]. The reducing ends of the liberated *N*-glycans were labeled with a fluorophore, 2-aminopyridine, by reductive amination [16]. The excess reagents were removed by phenol–chloroform extraction and cation-exchange chromatography [17]. The resulting PA-*N*-glycans were further purified by normal phase HPLC according to the method of Nakakita et al. [18] with minor modifications. Briefly, the lyophilized PA-*N*-glycans were dissolved in water and then injected into a TSKgel Amide-80 column (4.6 × 75 mm, Tosoh, Tokyo, Japan). The solvents used were

Table 1
Structures and elution positions in HPLC of standard PA-oligosaccharides

Abbreviation	Structure	Elution position in HPLC	
		RP (GU)	NP (GU)
ag22bis	GlcNAcβ1-2Manα1$_{\backslash 6}$ GlcNAcβ1-4Manβ1-4GlcNAcβ1-4GlcNAc-PA GlcNAcβ1-2Manα1$^{/3}$	11.45	5.37
22bis	Galβ1-4GlcNAcβ1-2Manα1$_{\backslash 6}$ GlcNAcβ1-4Manβ1-4GlcNAcβ1-4GlcNAc-PA Galβ1-4GlcNAcβ1-2Manα1$^{/3}$	12.72	6.78
ag22bisF	GlcNAcβ1-2Manα1$_{\backslash 6}$ Fucα1$_{\backslash 6}$ GlcNAcβ1-4Manβ1-4GlcNAcβ1-4GlcNAc-PA GlcNAcβ1-2Manα1$^{/3}$	14.90	5.66
$G_1$22bisF	Galβ1-4GlcNAcβ1-2Manα1$_{\backslash 6}$ Fucα1$_{\backslash 6}$ GlcNAcβ1-4Manβ1-4GlcNAcβ1-4GlcNAc-PA GlcNAcβ1-2Manα1$^{/3}$	15.86	6.29
22bisF	Galβ1-4GlcNAcβ1-2Manα1$_{\backslash 6}$ Fucα1$_{\backslash 6}$ GlcNAcβ1-4Manβ1-4GlcNAcβ1-4GlcNAc-PA Galβ1-4GlcNAcβ1-2Manα1$^{/3}$	16.80	7.02
224F	Galβ1-4GlcNAcβ1-2Manα1$_{\backslash 6}$ Fucα1$_{\backslash 6}$ Galβ1-4GlcNAcβ1$_{\backslash 4}$ $^{\backslash 6}_{\backslash 3}$Manβ1-4GlcNAcβ1-4GlcNAc-PA Galβ1-4GlcNAcβ1$^{/2}$Manα1$^{/3}$	13.91	7.96

(A) 90% acetonitrile–3% acetic acid titrated to pH 7.3 with triethylamine and (B) 20% acetnitrile–3% acetic acid titrated to pH 7.3 with triethylamine. Elution was performed at a flow rate of 1.0 ml/min at 40 °C. The column was equilibrated with solvent A, and after injection of a sample, the following gradient was employed: 0–28% B over 7 min; 28–100% B over 5 min; 100% B for 4 min. PA-*N*-glycans were detected with a fluorescence spectrophotometer using excitation and emission wavelengths of 310 and 380 nm, respectively. The fraction between 7 and 16 min after the injection was collected, concentrated, and used for the structural studies.

Preparation and size-fractionation of asialo-PA-N-glycans. PA-*N*-glycans were dissolved in 50 μl of 100 mM ammonium acetate buffer (pH 5.0) and then digested with 2 U/ml of *Arthrobacter ureafaciens* neuraminidase (Nacalai Tesque, Kyoto, Japan) at 37 °C for 24 h. The reaction was terminated by boiling for 3 min, followed by centrifugation at 13,000*g* for 10 min. The resulting supernatant was injected into a normal phase HPLC apparatus equipped with a TSKgel Amide-80 column (4.6 × 75 mm), and the asialo-PA-*N*-glycans were size-fractionated into nine fractions from glucose unit (GU) 3 to GU12 at intervals of one glucose unit, according to the method of Fujimoto et al. [19] with some modifications. The solvents used were (A) 90% acetonitrile–0.6% acetic acid titrated to pH 7.3 with triethylamine and (B) 20% acetnitrile–0.6% acetic acid titrated to pH 7.3 with triethylamine. The elution was performed at 40 °C using a flow rate of 1 ml/min. The column was equilibrated with 5% solvent B, and after injection of a sample, solvent B was increased linearly to 75% in 25 min. The PA-*N*-glycans were detected using excitation and emission wavelengths of 310 and 380 nm, respectively.

HPLC for structural analysis. Reversed phase HPLC was performed at 30 °C on a Cosmosil $3C_{18}$-P column (2 × 100 mm, Nacalai Tesque) at a flow rate of 0.2 ml/min. The solvents used were (A) 20 mM ammonium acetate buffer pH 4.0 and (B) the same buffer containing 0.5% 1-butanol. The column was equilibrated with 5% solvent B, and after injection of a sample, solvent B was linearly increased to 100% over 50 min and then held at 100% for 3 min. Fluorescence was monitored using excitation and emission wavelengths of 320 and 400 nm, respectively.

Normal phase HPLC was performed at 40 °C on a TSKgel Amide-80 (2 × 150 mm, Tosoh) at a flow rate of 0.2 ml/min. The solvents used were (A) 90% acetonitrile–0.6% acetic acid titrated to pH 7.3 with triethylamine and (B) 20% acetnitrile–0.6% acetic acid titrated to pH 7.3 with triethylamine. The column was equilibrated with 5% solvent B, and after injection of a sample, solvent B was linearly increased to 75% over 40 min. Fluorescence was monitored using excitation and emission wavelengths of 310 and 380 nm, respectively.

The structures of the PA-glycans were assessed by two-dimensional sugar chain mapping [20–22]. The retention time of each of PA-glycans was given in glucose unit based on the elution time of the PA-isomaltooligosaccharides. The behavior of authentic PA-oligosaccharides on HPLC is shown in Table 1.

Glycosidase digestion for structural analysis. PA-glycans were digested in a volume of 20 μl for 16 h at 37 °C using the following enzymes: *Streptococcus pneumoniae* β-galactosidase (Prozyme, San Leandro, CA), specificity for β(1,4)Gal, 0.1 U/ml in 50 mM sodium acetate buffer, pH 5.6; *Streptomyces* sp.142 α-fucosidase (Takara), specificity for α(1,3/4)Fuc, 0.2 mU/ml in 50 mM potassium phosphate buffer, pH 6.0.

NanoESI ion-trap mass spectrometry. Mass spectra of the PA-glycans were observed on a Finnigan LCQ Deca XP ion-trap mass spectrometer (Thermo Electron Co., Waltham, MA) equipped with a nanoESI device (AMR, Inc., Tokyo, Japan) connected to a Paradigm MS4 μHPLC system (Michrom BioResources, Inc., Auburn, CA). Reversed phase HPLC was performed at room temperature on a Magic C18 column (5 μm, 0.2 × 50 mm, Michrom BioResources) with a FortisTip capillary needle (AMR, Inc.) at a flow rate of 2 μl/min. The solvents used were (A) 5 mM acetic acid titrated to pH 6.0 with triethylamine and (B) 50% (v/v) methanol. The column was pre-equilibrated with solvent A, and 3 min after injection of a sample, solvent B was increased to 100% over 1 min and then held at 100% for 10 min. The nanoESI voltage was set at 1.8 kV and the capillary temperature was 200 °C.

Results

Tissue preparation for LMD

Hematoxylin and eosin (H&E) are the most commonly used histochemical stains. Good recovery (85%) of pyridylamino (PA) *N*-glycans was obtained after H&E

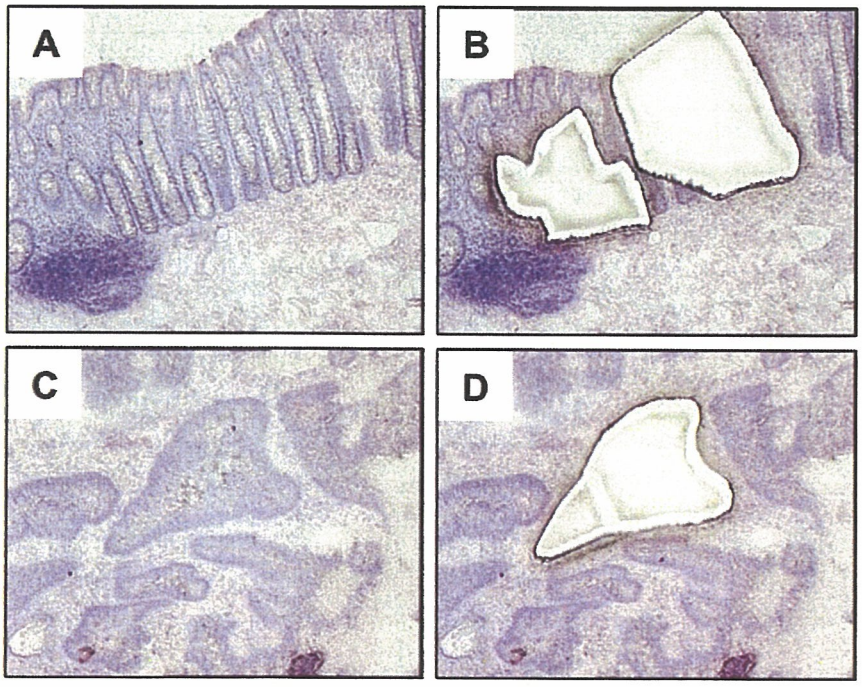

Fig. 1. Photomicrographs of laser microdissection of H&E stained tissue sections of normal colon (A,B) and cancerous colon (C,D). (A,C) Normal colon and cancerous colon, respectively, before microdissection. (B,D) Samples after successful microdissection. Representative data are shown.

staining and solubilization of the sections with 50% hexafluoroisopropanol (HFIP)/0.1% acetic acid mixture. Moreover, there was no gross effect on the resulting asialo-PA-*N*-glycans profile of colon cancer tissues (Supplementary Fig. 1). Thus, H&E staining and HFIP/acetic acid mixture were used for tissue preparation prior to LMD and for solubilization of samples, respectively. Colon cancer cells and normal colonic epithelial cells were successfully microdissected with the laser from the tumor and normal tissue sections, respectively, as shown in Fig. 1.

Comparison of N-glycan profiles from the LMD- and the bulk tissue-derived samples

PA-*N*-glycans were prepared from the LMD- or the bulk tissue-derived samples. After sialidase digestion, the resulting asialo-PA-*N*-glycans were separated into nine fractions (F1–F9) by normal phase HPLC (Fig. 2), in which oligosaccharides were separated in accordance with their molecular size. Each of the collected fractions was further separated by reversed phase HPLC. Comparison of the *N*-glycan profiles obtained from the LMD-derived samples with those from the bulk tissue-derived samples showed clear differences in fractions F2–F6 (Fig. 3). Although the expression profile of many *N*-glycans is different between normal and cancerous cells, we picked up 12 characteristic peaks (G1–G12) whose marked expression changes could only be detected using the LMD procedures. The detection of these peaks directly demonstrates the potential of using LMD to overcome problems associated with tissue heterogeneity. All 12 peaks displayed a substantial decrease in intensity in the cancerous colon cells relative to normal colon cells. Each of these peaks was fractionated and further purified by normal phase HPLC for structural analysis as described in Materials and methods. Elution positions of G1–G12 on normal and reversed phase HPLC are summarized in Fig. 4A as a two-dimensional map. Peaks G3, G5, G10, and G12 had the same positions on the map as G2, G4, G6, and G9, respectively, indicating that each paired peak possessed the same structure. These results presumably arose from incomplete separation during the initial size-fractionation step (Fig. 2). From the positions on the map corresponding to authentic PA-*N*-glycans (Table 1), G1, G2 (G3), G4 (G5), G6 (G10), and G9 (G12) were estimated to be ag22bis, ag22bisF, $G_1$22bisF, 22bisF, and 224F, respectively. These structures were also confirmed by mass analysis (Table 2). The structures of the peaks G7, G8, and G11 were determined by two-dimensional mapping combined with exoglycosidase digestion and mass spectrometry as follows.

Peaks G7 and G8, both of which had the same composition of $Hex_5HexNAc_5dHex_2$-PA (Table 2), were sequentially digested with exoglycosidases in following order: 1st *S. pneumoniae* β(1,4)-galactosidase, *S.* sp142 α(1,3/4)-fucosidase, and 2nd *S. pneumoniae* β(1,4)-galactosidase (Fig. 4B and Supplementary Table 1). A single residue was removed at each step, indicating the presence of one Lewis^x structure with fucose linked α(1,3) to GlcNAc (the presence of fucose rendering the galactose residue resistant to cleavage). Elution positions on the map of the digests were shifted to that corresponding to the authentic PA-*N*-glycans, $G_1$22bisF and ag22bisF, after digestion with the α-fucosidase and

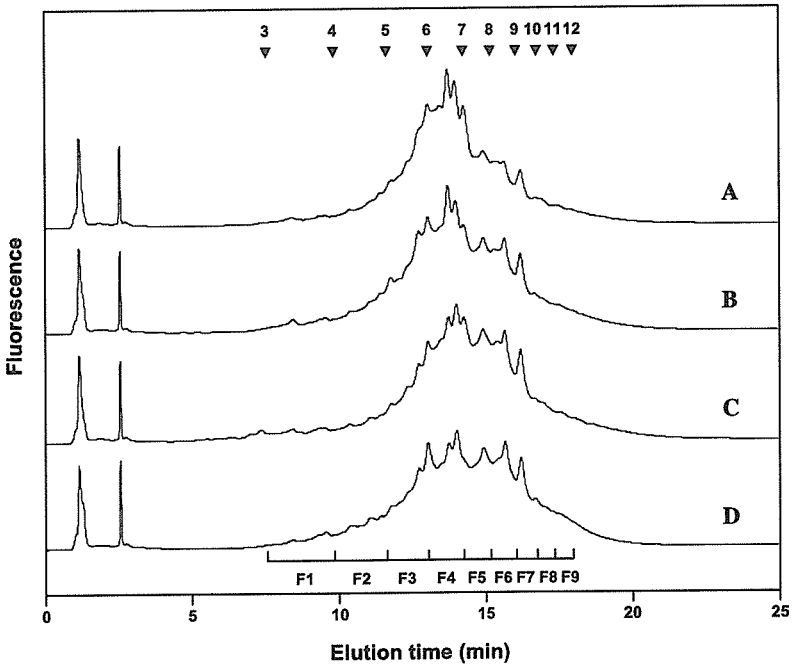

Fig. 2. Size-fractionation HPLC of asialo-PA-*N*-glycans from normal colon and colon cancer. (A,B) Normal and cancerous colon, respectively, which were not subjected to laser microdissection (LMD). (C,D) Normal and cancerous colon, respectively, which have been subjected to LMD to isolate normal epithelial cells and tumor cells. Numbered arrowheads indicate the elution position of PA-isomaltooligosaccharides with the corresponding degree of polymerization. Fractions F1–F9 were collected as indicated by the partitioned bars.

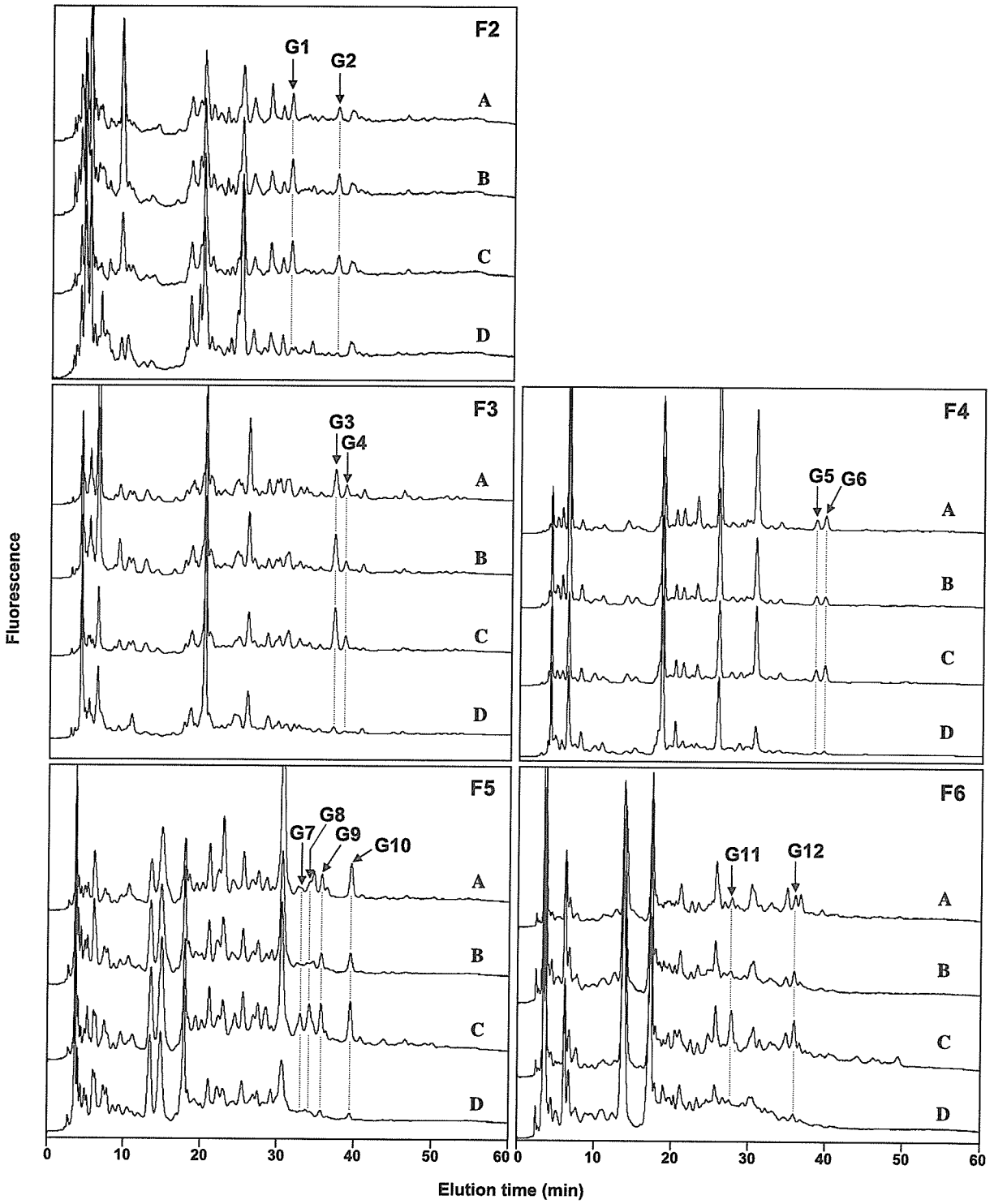

Fig. 3. Reversed phase HPLC profiles of the fractions F2–F6. (A,B) Normal and cancerous colon, respectively, which were not subjected to laser microdissection (LMD). (C,D) Normal and cancerous colon, respectively, which have been subjected to LMD. Twelve peaks (G1–G12) were collected.

the 2nd β-galactosidase, respectively. Thus the structures of these two peaks were estimated to be 22bisF with one Lewis^x structure.

Peak G11, which had the composition of $Hex_5HexNAc_5dHex_3$-PA (Table 2), was resistant to digestion with *S. pneumoniae* β(1,4)-galactosidase, but was sensitive to sequential digestion with *S.* sp142 α(1,3/4)-fucosidase followed by *S. pneumoniae* β(1,4)-galactosidase (Fig. 4B and Supplementary Table 1). Two residues were removed at each step indicating the presence of the two Lewis^x structures with fucose linked α(1,3) to GlcNAc. Elution positions on the map of the digests were shifted to that corresponding to the authentic PA-*N*-glycans, 22bisF and ag22bisF, after digestion with the α-fucosidase and the

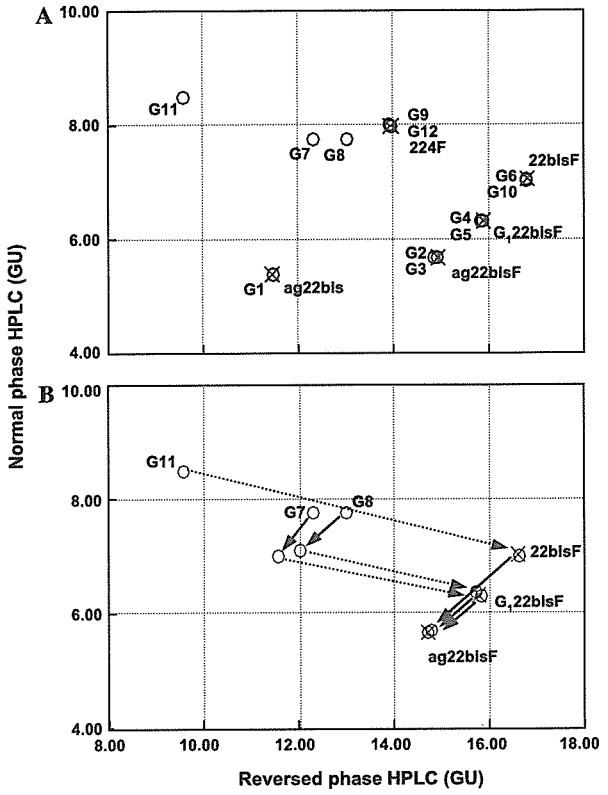

Fig. 4. Two-dimensional map of the PA-*N*-glycans. The elution profiles of each PA-*N*-glycan on normal and reversed phase HPLC were expressed in glucose units (GU) based on the elution times of the PA-isomaltooligosaccharides and plotted on the map. (A) Map of peaks G1–G12. (B) Map of the sequential exoglycosidase digests of peaks G7, G8, and G11. Circles indicate the positions of the each peak. X indicates the position of the standard PA-*N*-glycan. Solid arrows indicate the direction of change in the elution positions after digestion with β1,4-galactosidase. Dotted arrows indicate the direction of change in the elution position after digestion with α1,3/4-fucosidase.

Table 2
Mass analysis of the PA-*N*-glycans G1–12

Peak	Mass		Estimated composition
	Observed	Calculated	
G1	1598.2	1598.6 $[M+H]^+$	$Hex_3HexNAc_5$-PA
G2	1744.3	1744.7 $[M+H]^+$	$Hex_3HexNAc_5dHex_1$-PA
G3	1744.2	1744.7 $[M+H]^+$	$Hex_3HexNAc_5dHex_1$-PA
G4	1906.2	1906.7 $[M+H]^+$	$Hex_4HexNAc_5dHex_1$-PA
G5	1906.2	1906.7 $[M+H]^+$	$Hex_4HexNAc_5dHex_1$-PA
G6	2069.1	2068.8 $[M+H]^+$	$Hex_5HexNAc_5dHex_1$-PA
G7	2215.1	2214.9 $[M+H]^+$	$Hex_5HexNAc_5dHex_2$-PA
G8	2213.9	2214.9 $[M+H]^+$	$Hex_5HexNAc_5dHex_2$-PA
G9	2229.8	2230.8 $[M+H]^+$	$Hex_6HexNAc_5dHex_1$-PA
G10	2068.5	2068.8 $[M+H]^+$	$Hex_5HexNAc_5dHex_1$-PA
G11	2359.7	2360.9 $[M+H]^+$	$Hex_5HexNAc_5dHex_3$-PA
G12	2230.2	2230.8 $[M+H]^+$	$Hex_6HexNAc_5dHex_1$-PA

β-galactosidase, respectively. Thus the structure of G11 was estimated to be 22bisF with two Lewis^x structures.

The estimated structures of PA-*N*-glycans G1–G12 are summarized in Table 3. One of the seven identified *N*-glycans is a triantennary complex-type *N*-glycan with core α(1,6) fucose residue, whereas the other six are derivatives of the bisecting GlcNAc-bearing complex-type *N*-glycans with or without Lewis^x α(1,3) and/or the core fucose residues.

Discussion

Tissue heterogeneity and the consequent need for enrichment of specific cell types before sample analysis presents a major problem in the study of cancer. The presence of contaminating cells within a sample hampers its accurate molecular analysis, and the results obtained cannot easily be traced back to the biological properties of the tumor itself. Acquisition of specific cell populations in sufficient quantity and quality is a substantial challenge. LMD is one of the methods that is being increasingly used to overcome this problem, and has already been extensively employed for the analysis of DNA, RNA, and protein.

In this study, we have investigated the potential of LMD as a tool in cancer glycomic studies using colon cancer as a model. First, we confirmed the preservation of *N*-glycan profiles after histological procedures, including alcohol fixation, H&E staining, PBS washing, and dehydration with alcohol, followed by solubilization with HFIP/acetic acid mixture (Supplementary Fig. 1). PA-*N*-glycans prepared from the microdissected tissue samples were of sufficient quality for structural analysis in the form of two-dimensional sugar chain mapping and ESI-MS. These findings demonstrated the feasibility of using LMD in combination with *N*-glycan analysis for the clinical evaluation of cancerous tissue samples.

In this study, we compared the profiles of *N*-glycans derived from LMD samples (new method) with those from the non-LMD samples (conventional method). Our analysis of the LMD samples readily identified seven characteristic *N*-glycans whose marked expression differences between normal and cancerous colon cells could only be detected using the LMD procedure (Fig. 3). By contrast, analysis of the bulk samples (conventional method) did not reveal such alterations in these *N*-glycans. This result clearly indicates the existence of cells-type specific expression of *N*-glycans in the tissue specimen that can be detected with the aid of LMD. Thus, our study has demonstrated the general utility of LMD in glycan analysis by overcoming problems associated with tissue heterogeneity.

In summary, to the best of our knowledge, this is the first application and evaluation of LMD in cancer glycomics. The usefulness of this technique was demonstrated by showing the existence of unique changes to the expression of *N*-glycans in cancerous colon cells that can only be detected using microdissected cell samples. We believe that the combination of LMD and glycomics will define changes in glycan expression patterns that occur with cancer development and progression, and thereby facilitate the identification of new molecular markers and/or potential therapeutic targets. However, further refinements of the LMD technology to permit more rapid and reliable procurement of a substantial amount of sample will be required.

Table 3
Estimated structures of PA-*N*-glycans G1–G12

Peak	Structure	Abbreviation	CC/NC ratio[a]	
			LMD (−)	LMD (+)
G1	GlcNAcβ1-2Manα1(6) GlcNAcβ1-4Manβ1-4GlcNAcβ1-4GlcNAc-PA GlcNAcβ1-2Manα1(3)	ag22bis	1.13	0.12
G2 (G3)	GlcNAcβ1-2Manα1(6) Fucα1(6) GlcNAcβ1-4Manβ1-4GlcNAcβ1-4GlcNAc-PA GlcNAcβ1-2Manα1(3)	ag22bisF	1.20	0.10
G4 (G5)	Galβ(1,4)$_1$ { GlcNAcβ1-2Manα1(6) Fucα1(6) / GlcNAcβ1-2Manα1(3) } GlcNAcβ1-4Manβ1-4GlcNAcβ1-4GlcNAc-PA	$G_1$22bisF	0.91	0.09
G6 (G10)	Galβ1-4GlcNAcβ1-2Manα1(6) Fucα1(6) GlcNAcβ1-4Manβ1-4GlcNAcβ1-4GlcNAc-PA Galβ1-4GlcNAcβ1-2Manα1(3)	22bisF	0.66	0.13
G7 and G8	Fucα(1,3)$_1$ Galβ1-4GlcNAcβ1-2Manα1(6) Fucα1(6) GlcNAcβ1-4Manβ1-4GlcNAcβ1-4GlcNAc-PA Galβ1-4GlcNAcβ1-2Manα1(3)	$(Le^x)_1$22bisF	0.74	0.09
G9 (G12)	Galβ1-4GlcNAcβ1-2Manα1(6) Fucα1(6) Galβ1-4GlcNAcβ1(6,3)Manβ1-4GlcNAcβ1-4GlcNAc-PA Galβ1-4GlcNAcβ1(4,2)Manα1	224F	0.92	0.22
G11	Fucα1(3) Galβ1-4GlcNAcβ1-2Manα1(6) Fucα1(6) GlcNAcβ1-4Manβ1-4GlcNAcβ1-4GlcNAc-PA Galβ1-4GlcNAcβ1-2Manα1(3) Fucα1(3)	$(Le^x)_2$22bisF	0.78	0.07

[a] Ratios were calculated from the peak areas on reversed phase HPLC in Fig. 3.

Acknowledgments

This work was supported in part by Grant-in-Aid for Scientific Research (C) No. 17510191 from the Ministry of Education, Culture, Sports, Science and Technology of Japan and by research grants from the Ministry of Health, Labour and Welfare of Japan.

Appendix A. Supplementary data

Supplementary data associated with this article can be found, in the online version, at doi:10.1016/j.bbrc.2006.10.191.

References

[1] A. Varki, Biological roles of oligosaccharides: all of the theories are correct, Glycobiology 3 (1993) 97–130.
[2] R.A. Dwek, Glycobiology: "towards understanding the function of sugars", Biochem. Soc. Trans. 23 (1995) 1–25.
[3] J.W. Dennis, M. Granovsky, C.E. Warren, Protein glycosylation in development and disease, Bioessays 21 (1999) 412–421.
[4] A. Kobata, A journey to the world of glycobiology, Glycoconj. J. 17 (2000) 443–464.
[5] D.H. Dube, C.R. Bertozzi, Glycans in cancer and inflammation–potential for therapeutics and diagnostics, Nat. Rev. Drug Discov. 4 (2005) 477–488.
[6] S. Hakomori, Tumor malignancy defined by aberrant glycosylation and sphingo(glyco)lipid metabolism, Cancer Res. 56 (1996) 5309–5318.
[7] S. Hakomori, Glycosylation defining cancer malignancy: new wine in an old bottle, Proc. Natl. Acad. Sci. USA 99 (2002) 10231–10233.
[8] M. Fukuda, Possible roles of tumor-associated carbohydrate antigens, Cancer Res. 56 (1996) 2237–2244.
[9] J.W. Dennis, J. Pawling, P. Cheung, E. Partridge, M. Demetriou, UDP-*N*-acetylglucosamine:α-6-D-mannoside β1,6 *N*-acetylglucosaminyltransferase V (Mgat5) deficient mice, Biochim. Biophys. Acta 1573 (2002) 414–422.

[10] M. Fukuda, Roles of mucin-type *O*-glycans in cell adhesion, Biochim. Biophys. Acta 1573 (2002) 394–405.
[11] R. Kannagi, M. Izawa, T. Koike, K. Miyazaki, N. Kimura, Carbohydrate-mediated cell adhesion in cancer metastasis and angiogenesis, Cancer Sci. 95 (2004) 377–384.
[12] Y. Zhang, I. Schmack, D.G. Dawson, H.E. Grossniklaus, A.H. Conrad, Y. Kariya, K. Suzuki, H.F. Edelhauser, G.W. Conrad, Keratan sulfate and chondroitin/dermatan sulfate in maximally recovered hypocellular stromal interface scars of postmortem human LASIK corneas, Invest. Ophthalmol. Vis. Sci. 47 (2006) 2390–2396.
[13] N. Hirota, K. Mizuno, Y. Goto, Cooperative α-helix formation of β-lactoglobulin and melittin induced by hexafluoroisopropanol, Protein Sci. 6 (1997) 416–421.
[14] S. Hess, F.J. Cassels, L.K. Pannell, Identification and characterization of hydrophobic *Escherichia coli* virulence proteins by liquid chromatography-electrospray ionization mass spectrometry, Anal. Biochem. 302 (2002) 123–130.
[15] S. Natsuka, S. Hase, Analysis of *N*- and *O*-glycans by pyridylamination, Methods Mol. Biol. 76 (1998) 101–113.
[16] A. Kondo, J. Suzuki, N. Kuraya, S. Hase, I. Kato, T. Ikenaka, Improved method for fluorescence labeling of sugar chains with sialic acid residues, Agric. Biol. Chem. 54 (1990) 2169–2170.
[17] K. Yanagida, S. Natsuka, S. Hase, A pyridylamination method aimed at automatic oligosaccharide analysis of N-linked sugar chains, Anal. Biochem. 274 (1999) 229–234.
[18] S. Nakakita, D. Ama, S. Natsuka, S. Hase, Analysis of oligosaccharide structures of glycoproteins in polyacrylamide gel, Anal. Biochem. 303 (2002) 206–209.
[19] I. Fujimoto, K.K. Menon, Y. Otake, F. Tanaka, H. Wada, H. Takahashi, S. Tsuji, S. Natsuka, S. Nakakita, S. Hase, K. Ikenaka, Systematic analysis of N-linked sugar chains from whole tissue employing partial automation, Anal. Biochem. 267 (1999) 336–343.
[20] N. Tomiya, J. Awaya, M. Kurono, S. Endo, Y. Arata, N. Takahashi, Analyses of N-linked oligosaccharides using a two-dimensional mapping technique, Anal. Biochem. 171 (1988) 73–90.
[21] Y. Makino, K. Omichi, S. Hase, Analysis of oligosaccharide structures from the reducing end terminal by combining partial acid hydrolysis and a two-dimensional sugar map, Anal. Biochem. 264 (1998) 172–179.
[22] T. Takemoto, S. Natsuka, S. Nakakita, S. Hase, Expression of complex-type *N*-glycans in developmental periods of zebrafish embryo, Glycoconj. J. 22 (2005) 21–26.

特集　構造生物学の現在と今後の展開

質量分析の可能性—未知生体分子の探索ツールとして

高尾敏文

生体は多種多様な分子の複雑な混合物であり，それぞれの分子は秩序正しく配置され，時間および空間軸で量変動や構造変化をしながら機能を発揮している。さらに，生体分子の複雑かつ巧妙な点は，一つの分子が微細な構造変化によって空間的配置を変えたり，相互作用する分子のレパートリーを変えたりすることにより，生理機能を発揮している点である。従って，それらを理解するには，複雑な生体分子の集合体を網羅的に調べ，そこに存在する全ての分子を同定，さらには，存在量や構造変化などを解析するということが重要である。多種多様な分子で構成される生体を一網打尽に解析できる方法は今のところない。また，生体という複雑系を考えると，そのようなことは到底かなう話ではない。しかし，現在の網羅的解析の方向を生んでいるのは，様々な生物種のゲノム塩基配列の決定を背景に，質量分析による蛋白質同定がハイスループットで簡便に行えるようになり，生命科学においてパラダイムシフトが起きたからにほかならない。現在では，蛋白質に留まらず，糖や脂質などの様々な生体分子の網羅的解析にも利用されるようになり，質量分析をフルに活用した“オーム”解析が盛んに行われるようになった。

どんな分析においても測定分解能と感度は分析技術の発展には欠かせない重要な要素である。前者は複雑な構造を解き明かす上で，後者は微量にしかない，例えば生体分子などを検出する上で重要である。質量分析も正にこの二つのポイントに集約される技術開発が盛んに行われてきた。特に，測定感度という点においては，まず試料を気化し，イオン化する必要があるわけだが，30年程前までは，一般に揮発しにくい生体分子はまったく測定の対象外であった。1980年代に入り，いくつかの画期的なイオン化法が開発されたことにより，分析対象は一挙に生体高分子にまで拡がり，測定感度は飛躍的に向上し，今や，アト(10^{-18})モル量の極微量試料でも測定の範疇に入るほどの高感度測定が可能となった。

現在市販されている質量分析計は，分析部の方式としては大きく分けて5種類ほどだが，市販機の種類となると，プロテオミクスに絞っても約30機種以上挙げられる。このように多様な機種が開発される理由の一つは質量分析の特殊事情にある。質量分析法は分子や原子を電場や磁場の中で直接操作し検出するという点で，ほかの分光学的な分析法とはまったく異なる原理に基づいている。従って，質量分析を行うには，まず，試料分子を真空中に気化，イオン化するという極めて困難なハードルを乗り越えなければならない。そしてさらに厄介なことは，効率よく気化，イオン化するためには，それに適した試料を導入してやる必要がある。すなわち，試料の前処理や分離という質量分析の前段階が測定の結果を大きく左右し，特に，微量試料の場合は測定の成否を握る。そのような理由から，市販機では液体クロマトグラフィーなどの分離技術との組み合わせをはじめとする様々な工夫がなされており，装置の多様化

Future of mass spectrometry—A tool for discovery of unknown biomolecules
Toshifumi Takao：大阪大学 蛋白質研究所 機能・発現プロテオミクス研究系(〒565-0871 吹田市山田丘3-2)

の一因となっている。

前述のように，難揮発性物質をイオンとして気化することは20世紀後半における質量分析の大きな命題であった。そのような中，1980年代半ばに相次いで報告された二つのイオン化法(エレクトロスプレーイオン化[1]とソフトレーザーイオン化法[2])は，特に生体高分子の測定を可能とし，2002年度のノーベル化学賞の対象にもなった。質量分析において，イオン化は生体試料のような微量試料に対しては測定の成否を握る極めて重要なポイントになるが，これら二つのイオン化法を駆使しても試料分子のほんの一部がイオン化しているにすぎず，近い将来，より高効率のイオン化法が出現するものと期待される。

生体には未だ検出されていない極微量の機能性分子や，疾患マーカーなどの生理機能はないが生理状態を反映する有用な分子があるものと考えられる。また，既知の分子においても，生体の中では発現量の変化やまだ知られていない微小な構造変化をしている可能性もある。それらを探索，解析する方法として，現状では，質量分析法は最も適した分析法といえるが，それには前述のように，質量分析に供するまでの試料の前処理や分離が極めて重要になってくる。最新の質量分析計を駆使すれば，“フェムトモルオーダーの試料量での測定がルーチンかつハイスループットで行える”とよくいわれる。しかし，実際の試料を質量分析にかける際には，大抵の場合，まず対象とする物質を濃縮あるいは分離したり，供雑物を除去したりする操作が必要となるため，どうしてもロスや分解は避けられず，フェムトモルオーダーの生体試料を出発材料として分析まで到達するのは極めて難しい。また，扱う試料の状態も，特に生体から得られるものは様々であり，一概に分析必要量を見積もるのは困難である。

以上のように，質量分析は多くの技術革新により，特に生物・医学の分野で大きく貢献，利用されるようになったが，今後その可能性を一層拡げるには，質量分析法の特性を熟知した上で，目的の物質群に照準を当てた試料前処理法や分離技術をいかに工夫するかということが重要になってくる。試料調製，分離法は，検出したい対象試料分子や出発材料に応じて最適な方法を確立する必要がある。言い換えれば，血液，尿，組織，細胞抽出物といった生体材料は，直接質量分析に供しても有意なデータを得るのは難しい。それらに対する前処理や分離法は，当然のことながら，ペプチド，蛋白質，あるいは糖鎖や脂質といった生体成分の何に照準を当てて分析するかによって異なり，また，目的に応じて最適化も必要となる。

実　例

生体材料を扱った質量分析による網羅的解析の一例として，われわれが現在取り組んでいる“尿中の蛋白質のプロファイリング”について紹介する。目的は，尿から早期診断や予後診断に有用な疾患マーカーを探索するためである[3]。尿を対象とした理由は，実際にヒトの生体材料として最も調達しやすいこと，蛋白質の分解がほかの生体材料と比較して少ないという点が大きな理由である。勿論，尿をそのまま質量分析にかけてもペプチドや蛋白質はほとんど見えない。ましてや，疾患マーカーとなりうる微量ペプチド・蛋白質は検出できないので，当初はまず，尿からペプチド・蛋白質を効率よく単離するところから始める必要があった。ここでは簡単に質量分析までの試料調製の流れと解析結果について述べる[4]。

図1に示したように，比較解析したい尿(ここでは妊娠中と出産後のヒトの尿)を別々に採取後，塩や色素などの低分子化合物を限外濾過により除き，得られた蛋白質溶液を乾固し，次に二つの試料間での量変動解析を行うために，それぞれの試料を通常の蒸留水で調製した緩衝液と^{18}O標識水($H_2{}^{18}O$)で調製した緩衝液に別々に溶解し，同条件で酵素消化を行った。得られたペプチド混合物を同量混合の後，ナノHPLCで分離，溶離液を直接MALDI-MS用のステンレス製のプレートに30秒毎に位置を変えながらブロットした(図2a，図3)。その後に，MALDI用マトリックスとして，α-シアノ-4-ヒドロキシ桂皮酸の溶液をそれぞれのスポットに添加し，乾燥後，図4に示すMALDIタンデム質量分析計を用いて測定した。それぞれの分画された試料スポットに対し，MS測定→分子質量と強度を取得→観測されたペプチ

a

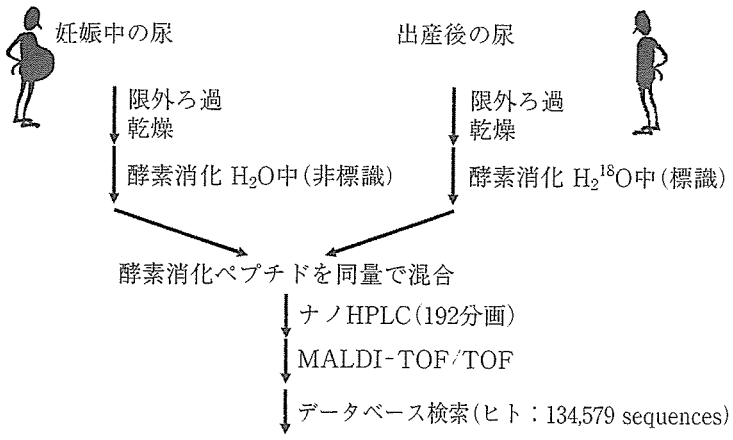

b

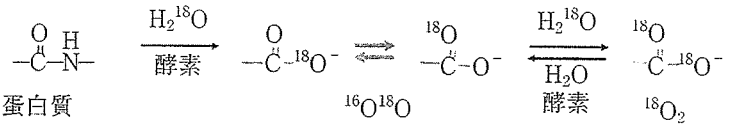

図1　a：ヒト尿蛋白質のプロファイリングと比較解析の流れ，b：酵素消化(加水分解)による^{18}O標識。＊ウェブアプリケーションIsotopica(http://coco.protein.osaka-u.ac.jp/Isotopica)を用いて，分子イオン領域に観測される$^{16}O_2$，$^{16}O^{18}O$，$^{18}O_2$の三つのイオン種のピーク強度比を算出(図2B，2C)

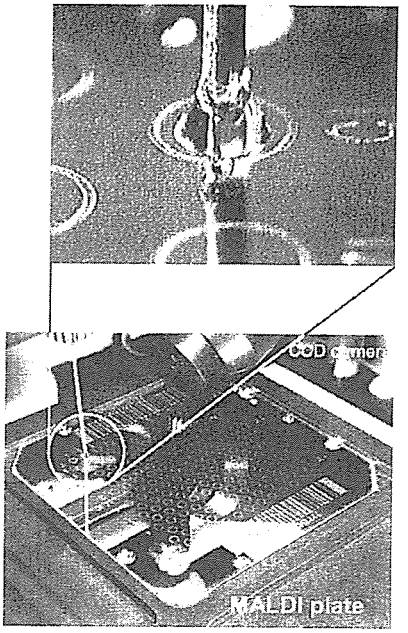

図3　ナノHPLCから溶出するペプチド溶液をMALDI-MS用のプレートにブロットする様子

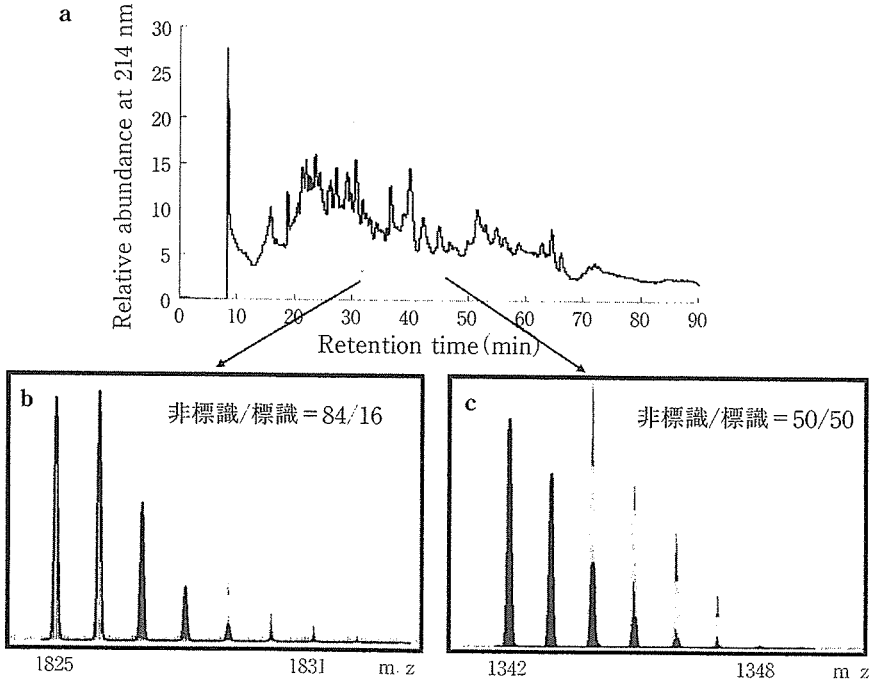

図2　妊娠中と出産後のヒト尿由来蛋白質の比較解析

a：別々に調製した妊娠中(非標識)および出産後(^{18}O標識)のヒト尿由来蛋白質のリシルエンドペプチダーゼ消化物の同量混合物のナノHPLC。b，c：二つの典型的なMALDI-MSスペクトルの分子イオン領域。各々のペプチドはMS/MSによりpoly-Ig receptor(B)，serum albumin(C)に帰属された。該当するアミノ酸配列と観測同位体分布をもとに非標識(青色のトレース)と標識(^{18}Oが1個[桃色]と^{18}Oが2個[黄色]導入された分子種の和)の比をIsotopicaにより算出。(巻頭カラー8頁)

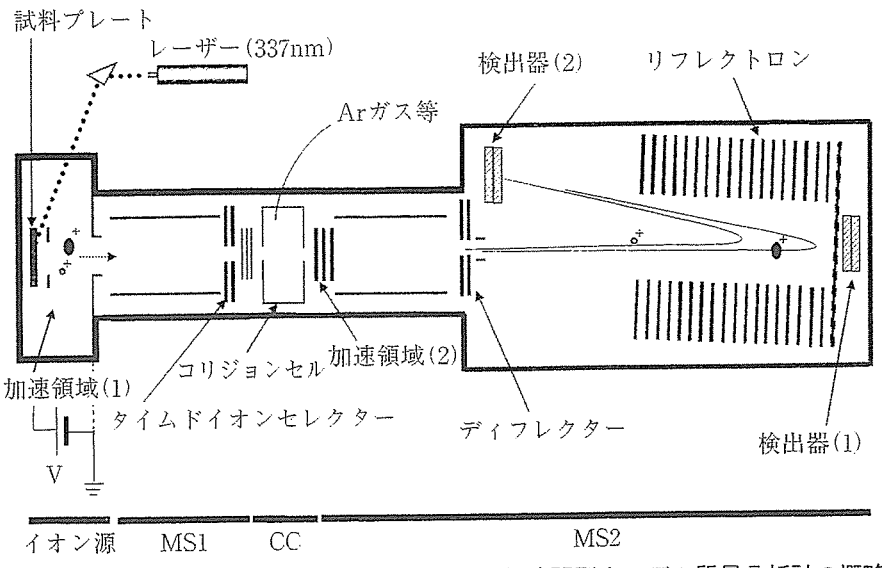

図4 マトリックス支援レーザー脱離イオン化飛行時間型タンデム質量分析計の概略図
飛行時間型質量分析計2台(MS1とMS2)をタンデムに連結した装置で，イオン化法としては紫外レーザー(337 nm)によるMALDIが採用されており，ハイスループットでの蛋白質同定に適している。この装置によるMS/MSでは，MS1で分離した特定のイオンをタイムドイオンセレクターにより選択し，引き続き，選択したイオンをコリジョンセル内で分解，そして，生成したフラグメントイオンを一定のエネルギーになるように再加速後，MS2-リフレクトロン(反射電場)で質量分析することができる。そのため，分解能，精度の点で優れた結果を与えてくれる。

ドイオンを前駆イオンとしてMS/MS測定という一連の動作を自動で行った。測定時間はスポットの数とスポットあたりの前駆イオンの数などによって異なるが，一つのMS/MS測定に要する時間は約10秒程度である。蛋白質の同定は，ヒトの配列データベース(134,579配列，2005年4月)に対して，測定した全てのMS/MSスペクトル(この分析では約500枚)をもとに行い，同定結果は自動で出力される。

ここで示した方法では，1回の採取の尿10 m*l*を出発材料として，逆相系のナノHPLC(90分の通常のグラジエント分析)による1回の分離で約50種類程度の蛋白質が同定された。出発材料を増やす，あるいは，異なる試料調製法や高度な分離法(例えばイオン交換と逆相系による二次元LC)を用いれば，同定される蛋白質の種類や数は増えるが，ここではまず，尿中に存在する主要な蛋白質の存在様式(種類と量)をみることとし，上述のような簡便な方法により分析を行っている。

さらに，二つの試料間での蛋白質の量変動解析に^{18}O標識法を利用した。すなわち，一方の試料は調製時に^{18}O標識を行い，もう一方は非標識下で調製し，両者を同量混合して分析を行った後に後述の方法により非標識/標識の比を求めることで蛋白質の量変動を解析した(図1a)。^{18}O標識法は蛋白質を酵素消化により断片化する際に簡単に行え(図1b)，生体試料の量変動解析にしばしば利用されるようになってきた。しかし，^{18}O標識による質量シフトは+2または+4uしかなく，天然同位体ピークと重なって観測されるために，最近まで標識，非標識のペプチドの量比を見積もるのは簡単ではなかった。われわれはこの問題を解決するために，新たにソフトウェア“Isotopica”を開発し[5,6]，WEB上での公開，利用も開始している[7]。このソフトウェアを利用すれば，実測されたペプチドの分子イオンをもとに，標識，非標識体の量比を正確に見積もることができる[8]。図2Cは血清アルブミン由来のペプチドだが，出産前後で変化はなく，ほぼ等量観測されている。それに対して図2bはpoly-Igレセプター由来ペプチドで，妊娠中では明らかに尿中に多く存在していることがわかる。

おわりに

質量分析計は感度，精度において性能は大幅に向上し，生命科学における優れた“探査機”となっ